UNIVERSITAT POLITÈCNICA DE CATALUNYA

DEPARTAMENT DE TEORIA DEL SENYAL I COMUNICACIONS

TESI DOCTORAL

HIGHER-ORDER STATISTICS APPLICATIONS IN IMAGE SEQUENCE PROCESSING

AUTOR : ELISA SAYROL CLOLS

DIRECTOR: ANTONI GASULL LLAMPALLAS

CHAPTER 4

MOTION ESTIMATION USING HIGHER-ORDER STATISTICS

In this chapter we propose a class of cost functions based on Higher-Order Statistics, to estimate the displacement vector between consecutive image frames. In case the sequence is severely corrupted by additive Gaussian noise of unknown covariance, using higher than second order statistics is appropriate since cumulants of Gaussian noise are zero. To obtain consistent cumulant estimates we need several records of the same sequence, which is not generally possible. Nevertheless, previous frames, where the registration problem has already been solved, can be used to obtain asymptotically unbiased estimates. This is possible when stationarity among the employed frames can be assumed. The objective of this work is to introduce HOS-based cost functions capable of estimating motion even for small regions or blocks. An alternative estimation is also provided, when only two frames are available, that outperforms other higher-order statistics-based cost functions. Finally, a recursive version to obtain the displacement is derived for cases when some a priori knowledge is available.

The chapter is organized as follows. The problem of motion estimation is introduced in Section 1. In Section 2 and 3, cost functions based on the variance and kurtosis of the displaced frame difference are revised and analytical expressions for AR models are developed. In section 4 a new class of HOS-based cost functions is derived and simulation and real results are given. In Section 5 a recursive version of the new cost function is presented and, finally, Section 6 is devoted to conclusions and final remarks.

4.1 Introduction

An image or video sequence is a series of 2-D images sequentially ordered in time. There is a growing interest in research applications involving image sequences, mainly in the area of image sequence analysis and image sequence processing. The latter refers to the operations of filtering, interpolation, subsampling and compression, which goals are the improvement of visual quality, conversion between video formats and bandwidth-efficient representation of image sequences [Sezan, 1993]. Image sequence analysis is aimed to those operations that generate some type of data for the purpose of information retrieval or interpretation [Huang, 1981a].

A lot of attention is focused on the estimation of 2-D motion or velocity field between successive frames. Its knowledge is useful in multiple areas involving not only analysis tasks such as segmentation and pattern recognition, but it is also helpful in processing tasks, for example motion estimation plays an important role in image compression and sampling structure conversion applications [Sezan, 1993]. Noise reduction is another example of image sequence processing that can benefit greatly from the knowledge of motion. There are some situations where the image sequence might be corrupted with noise, for example, images from surveillance cameras (which quality is often very poor) or medical images such as echographics with speckle noise. Assuming we know the position of an image point along a sequence, one-dimensional filtering can be applied through the direction of motion. This operation does not alter image features since the pixels are highly correlated along time (if not equal) and their grey levels do not change dramatically from frame to frame. On the other hand, noise is less correlated in time and even if it is colored its grey level may be quite different from frame to frame. Hence, by simply averaging or applying 1-D filters, such as median filters [Lagendijk, 1993], [Viero, 1993], noise may be drastically reduced.

4.1.1 Motion models

The computation of motion is an ill-posed inverse problem [Bertero, 1988], [Efstratiadis, 1991]. That is, (a) there is no solution for the data containing occlusion areas, (b) the solution satisfying the observed data is not unique, (c) there is a lack of continuity between data and solution since a slight modification of some intensity structures may cause significant change in the computation of the displacement vector, (d) on top of this, noise impedes the task of estimating motion.

All motion estimation algorithms involve additional assumptions about the motion structure. These assumptions may be represented implicitly or explicitly or, from another perspective,

motion can be defined by non-parametric or parametric models. An explicit formulation involves parametric motion models. In this case the problem of motion estimation reduces to that of estimating the values of the parameters. These models can be applied under limited circumstances, nevertheless highly accurate results may be obtained. Among these are Affine Flow models ; Planar Surface Motion under perspective projection models ; and Rigid Body Motion Models [Anandan, 1993]. On the other hand, when using non-parametric models some type of smoothness or uniformity constraint is imposed on the *local* variation of motion. As it might be expected, the results are limited in accuracy, but the model is applicable to a wide range of circumstances. Another interesting point of view arises from considering *local* or *global* models. The former constraints the motion in the neighborhood of a pixel whereas global models describe motion over the entire visual field. Parametric models are usually global models and non-parametric models are local.

4.1.2 A brief review of Motion Estimation Approaches

The methods for the estimation of the perceived motion may be classified into the following categories (according to [Efstratiadis, 1991]):

1) Histogram or segmentation-based methods. Some of the early work on motion estimation was the gradient transform method proposed by Fennema & Thomson [1979] based on a histogram identification. Several segmentation methods have also been proposed to estimate motion [Driessen, 1989], [Wu, 1990]. For example in [Cheong, 1993], images are segmented from the zero-crossings of the wavelet transform. This result is then used to extract moving objects.

2) Transform domain methods. In this case, motion is detected on the interframe changes in the transform domain. The Fourier transform and its shift property are frequently used [Huang, 1981b]. In [Kojima, 1993], the 3D FFT-Spectrum is used to detect the velocity of a moving object which spectrum lies in several planes of the frequency domain. The velocity is estimated by detecting the orientation of those planes. This type of methods, however, works well only in estimating the translation of moving objects and they are not effective in distinguishing multiple moving objects.

3) Region or feature matching algorithms. They are designed to produce a solution vector by finding the correspondence between structures in subsequent images. Once these structures are identified then the corresponding structure in the following images are searched by a certain optimization criteria. According to the region- or block-matching approach, the displacement vector at each pixel maximizes a similarity function or

minimizes an error function which is computed using small blocks that belong to successive frames. Such approaches maximize the correlation function [Bergmann, 1982], minimize the mean-squared error [Jain, 1981a] or the mean of the absolute frame difference [Srinivasan, 1985]. A kurtosis matching criteria has also been defined in [Anderson, 1991]. A recent work in this context is developed by Zhen and Blostein [1993], where a matching error weighting algorithm is employed for motion field estimation by adaptively modifying a regularization functional.

4) Spatio-temporal gradient methods. These were first introduced by Limb and Murphy [1975] and Cafforio and Rocca [1976]. Later, Netravali & Robbins [1980] motivated one of the most important applications of motion estimation, namely, the motion compensated coding of image sequences, by defining an efficient pixel-recursive gradient-based algorithm. This method minimizes the displaced frame difference function in a small causal area around the working point assuming constant image intensity along the motion trajectory. Anderson & Giannakis developed a pixel-recursive algorithm by minimizing a mean fourth-order cumulant criterion [1992].

5) Statistical methods. In this line, several algorithms have been proposed. A Maximum Likelihood formulation was presented by Martínez [1988] based on the direct form of the motion model and the Expectation Maximization algorithm was employed for the estimation of motion. In [Namazi, 1992], the generalized ML algorithm estimates the Karhunen-Loève expansion coefficients to search for the motion vector. Other authors have proposed a Bayesian Formulation. In [Konrad,1988] motion is modeled as a vector Markov random field and a Maximum A Posteriori probability criteria is derived to obtain the motion vector. Stiller [1993] addresses a model-based object-oriented motion estimator. The Displaced Frame Difference (DFD) is considered to obey a white generalized Gaussian distribution. A MAP estimator with respect to the image model is derived to estimate motion.

4.1.3 Motivation of the proposed Motion Estimator

The goal of this work is to estimate motion when image sequences are corrupted with noise. The final objective might be noise reduction in image frames. In this case and as we mentioned, we take advantage of the fact that image features are highly correlated as compared to noise samples along motion trajectories. Motivated by this fact, we consider finding the direction of motion, or in other words, solving first the registration problem and, in a second step, perform frame averaging, which is optimal in the maximum-likelihood sense. Observe that this approach is opposed to the reconstruction algorithms that exploit

the shift invariance property of cumulants as in the restoration schemes presented in the previous chapter. There, averaging was done in a higher-order domain and the shift was the same for all pixels.

We might be in a different situation, where the final goal is not to reduce noise but to estimate motion itself. For example, for analysis purposes, as is the case of noisy image sequences of the human heart which are of interest in assessing motility of the heart. In any case, whatever the final goals are, estimate motion is our prime objective.

We consider that no occlusions occur, that is, pixels of regions are visible over the entire frame and pixels do not move in or out of the images.

The reasons for choosing a motion model to fit in a given detection scheme are generally quite intuitive. We have chosen a non-parametric approach where the displacement vector is computed from the information in a local area. The reason is simply to allow a wider range of situations and not restrict ourselves to a particular motion model.

On the other hand, noise can be realistically described as a colored Gaussian process. In such circumstances, the study of Higher-Order Statistics of images may offer some advantages. As it was explained in chapter 2 cumulants can draw non-Gaussian signals out of Gaussian noise. Therefore, considering the statistics of the group of pixels under analysis to be non-Gaussian distributed allows to extract information of regions and its motion. Stationarity of the noise and signals is assumed among the employed frames.

Given the previous rationale we propose a motion estimation scheme that is divided in two steps, the second of which we concentrate our efforts :

Segmentation We may work with motion estimation based on blocks or on a segmentation approach. The latter aims to adapt the segmentation to the scene such that each region uniquely corresponds to one continuously moving 2-D object. Several problems that are inherent to block-oriented approaches are avoided, i.e., blocking artifacts are drastically reduced and small region sizes are not imposed. However the method becomes increasingly complex as the number of regions undergoing different displacements increases. There might be other statistical advantages or disadvantages in using one or the other approach. The size of blocks may be generally not too large in the block-matching approach. For example, in the H261 coding standard, blocks are taken to be 16x16 pixels in the lower level of the hierarchical block-matching step [CCITT, 1990]. This fact and the fact that pixels of one block may belong to different regions causes the block to be of Non-Gaussian statistics distribution. On the other side, pixels belonging to a same region are usually

considered Gaussian, specially for large and seemingly homogeneous regions. However, this is not true for textured regions which are often characterized by Non-Gaussian statistics. Since it is intended to apply methods that assume that regions are not normal distributed, a check of the Gaussianity should be carried out beforehand if possible. Otherwise any HOS-method fails to distinguish between the Gaussian statistics of the noise and the Gaussian statistics of the regions or blocks.

Motion estimation. For every moving region or block, we estimate motion using a cost function, that we also call performance index, that is maximized or minimized for the desired displacement. We are interested in choosing a cost function based on HOS to reduce the effect of colored Gaussian noise in our estimates. We define a criterion based on the minimization of a HOS function of the displaced frame difference.

According to the previous classification, the above approach might be considered to be a region or block matching method which recursive version (that will be defined at the end of the chapter) may be categorized into a spatio-temporal gradient method. The feature we are matching is the image intensity in a local area (that is represented by a block or segmented region).

4.1.3 Problem Formulation

From an image registration point of view, the problem of motion estimation can be stated as follows: "*given an image sequence, compute a representation of the motion field that best aligns pixels in one frame of the sequence with those in the next*"[Netravali, 1979]. This can be formulated as :

$$g_{k-1}(\boldsymbol{m}) = f_{k-1}(\boldsymbol{m}) + n_{k-1}(\boldsymbol{m})$$

$$g_k(\boldsymbol{m}) = f_k(\boldsymbol{m}) + n_k(\boldsymbol{m}) = f_{k-1}(\boldsymbol{m}-d_k^{\,o}(\boldsymbol{m})) + n_k(\boldsymbol{m}), \qquad (4.1)$$

where $\boldsymbol{m} = (m,n)$ denotes spatial image position of a point, $g_k(\boldsymbol{m})$ and $g_{k-1}(\boldsymbol{m})$ are observed image intensities at instant k and $k-1$, respectively, $f_k(\boldsymbol{m})$ and $f_{k-1}(\boldsymbol{m})$ are noise-free frames, $n_k(\boldsymbol{m})$ and $n_{k-1}(\boldsymbol{m})$ are assumed to be stationary, zero-mean Gaussian noise with unknown temporal and spatial covariance, and $d_k^{\,o}(\boldsymbol{m})$ is the displacement vector of the pixel of coordinates $\boldsymbol{m}$ during the time interval $[k-1,k]$. The noise-free frames are assumed to be zero-mean non-Gaussian signals which are statistically independent of the noise.

As mentioned in Chapter 2 a relationship between motion and image sequence should be established, it was assumed that image intensity was held constant along trajectories. This relationship was expressed as :

$$f_k(m) = f_{k-1}(m-d_k^o(m)), \tag{4.2}$$

This basic assumption is known as *Intensity Constancy Equation* and we have already substituted it in Eq. (4.1). The problem is to estimate $d_k^o(m)$ from the observation of $g_k(m)$ $g_{k-1}(m)$, and, in case it is possible, from other previous frames.

The $DFD_k(d)$, displaced frame difference, was first defined by Netravali & Robbins [1979] as

$$DFD_k(d) = g_k(m) - g_{k-1}(m-d) \tag{4.3}$$

where we omit the space dependency of the displacement to simplify notation. The $DFD_k(d)$ is defined in term of two quantities : (i) the spatial location; (2) and the displacement d with which it is evaluated. The $DFD_k(d)$ or other related functions, such as its correlation, its kurtosis or its gradient are obtained on every moving pixel.

Next, we introduce different criteria to obtain the displacement vector based on the $DFD_k(d)$. We analyze under which conditions it is more appropriate to utilize each of the cost functions. It is necessary to investigate the behavior of the cost functions for different displacements and SNR. For this purpose we use first-order AR models for the noise and the signal. These models are often utilized in Image Processing [Jain], with applications in data compression, image restoration, texture analysis and synthesis, and in several other situations. Here, they will be used to derive exact analytical expressions that will characterize cost functions under ideal circumstances. This is why in the following sections a rigorous study of the cost functions is carried out going beyond a mere ad hoc test that often leads to inconsistent results. Analytical expressions are derived for each performance index as a function of the correlation and higher-order moments of the image region and of the noise. We consider the cost functions for the case of correlation among pixels within a region as well as for the case of complete uncorrelation of pixels.

4.2 Variance of the DFD

A classical solution to obtain the displacement vector is the minimum square error [Netravali, 1979], which in terms of the $DFD_k(d)$ becomes:

$$J_{2k}(d) = E\{DFD_k{}^2(d)\} \tag{4.4}$$

$$\hat{d}_k^o <- min(J_{2k}(d))$$

A consistent estimation of this cost function is given by:

$$\hat{J}_{2k}(d) = \frac{1}{N} \sum_{m \varepsilon \Omega_m} DFD_k^2(d) \tag{4.5}$$

where Ω_m denotes the spatial domain that contains the pixels of a given region or block and N the number of such pixels.

From Eq. (4.3) and Eq. (4.1) we rewrite the *DFD* as:

$$DFD_k(d)=[f_k(m)+n_k(m)]-[f_{k-1}(m-d)+n_{k-1}(m-d)]$$

Defining the displaced signal difference as:

$$DSD_k(d) = f_k(m)-f_{k-1}(m-d)$$

and the displaced noise difference as:

$$DND_k(d) = n_k(m)-n_{k-1}(m-d),$$

we derive the DFD as a function of signal and noise differences:

$$J_{2k}(d) = E\{DSD_k^2(d)\} + E\{DND_k^2(d)\}$$

where we assumed that the noise is independent of the signal, then

$$J_{2k}(d) =2\sigma_f^2-2E\{f_k(m)f_{k-1}(m-d)\} + 2\sigma_n^2-2E\{n_k(m)n_{k-1}(m-d)\} \tag{4.6}$$

where

$$\sigma_n^2= E\{n_k(m)n_k(m)\} = E\{n_{k-1}(m-d)n_{k-1}(m-d)\}$$

on one hand and

$$\sigma_f^2 = E\{f_k(m)f_k(m)\} = E\{f_{k-1}(m-d)\, f_{k-1}(m-d)\}$$

on the other hand. We define the spatial-temporal covariance of the noise as:

$$r_{np}(d) = E\{n_k(m)n_{k-p}(m-d)\},$$

and we denote the spatial covariance of the signal by:

$$r_f(d_k^o - d) = E\{f_k(m) f_k(m + d_k^o - d)\}.$$

The intensity constancy Equation, Eq. (4.2), can be rewritten as:

$$f_{k-1}(m-d) = f_k(m + d_k^o - d). \tag{4.7}$$

Substituting the above equation into Eq. (4.6) the cost function can be expressed as a function of the covariances, therefore:

$$J_{2k}(d) = 2\sigma_f^2 - 2r_f(d_k^o - d) + 2\sigma_n^2 - 2r_{n1}(d). \tag{4.8}$$

This is the general expression that characterizes the second-order statistics-based cost function. From this equation particular expressions are derived depending on the nature of the noise and on the signal and noise models. Thus, in first place, we distinguish the cases of white and colored noise. Assuming noise is white in time the noise covariance is given by:

$$r_{n1}(d) = \sigma_n^2 \, \delta(k-(k-1)) = 0,$$

where $\delta(k)$ is the Kronecker delta. In this case

$$J_{2k}(d) = 2\sigma_f^2 + 2\sigma_n^2 - 2r_f(d_k^o - d))$$

which minimum does not depend on the noise. Thus, in case images are affected by white noise, the above cost function can be utilized to detect the correct displacement since the only noise contribution in Eq. (4.8) is the variance term which is assumed constant.

However, we are interested in studying the case when noise is colored, in which case its covariance is different from zero. In this situation the cost function at the correct displacement may not be a minimum. The characterization of the signal and noise covariances may allow a deeper knowledge of the effects of the degradation. This information may lead to the true displacement even though the signal is corrupted by colored noise. Following is an analytical study of $J_{2k}(d)$ when the covariance functions are described by AR models.

4.2.1 Study for Uncorrelated Region and Colored Noise

We start with a simpler case when the signal covariance is white. Although this is a very unlikely situation in image processing applications, it gives a better understanding of the behavior of the cost functions. On the other hand, colored noise can be characterized by the output of an IIR system excited by white noise:

$$H(z_m, z_n, z_k) = (1-a_m z_m^{-1})^{-1}(1-a_n z_n^{-1})^{-1}\,(1-a_k z_k^{-1})^{-1} \tag{4.9}$$

Since the transfer function H is separable, the covariance can be factored as [Jain, p. 214]:

$$r_{nl}(\boldsymbol{d}) = r_{nl}(d_m, d_n) = \sigma_n^2\, a_m^{|d_m|}\, a_n^{|d_n|}\, a_k \tag{4.10}$$

where the displacement has been decomposed into its two spatial components $\boldsymbol{d} = (d_m, d_n)$ and a_k is the AR temporal coefficient which appears to the power of one, since this is the temporal difference considered between two consecutive frames.

For an uncorrelated region, the covariance is zero except at the origin, that is for $\boldsymbol{d} = \boldsymbol{d}_k^o$. Thus Eq. (4.8) becomes

$$J_{2k}(\boldsymbol{d}) = 2\sigma_f^2\,(1-\delta(\boldsymbol{d}-\boldsymbol{d}_k^o)) + 2\sigma_n^2(1- a_m^{|d_m|}\, a_n^{|d_n|}\, a_k) \tag{4.11}$$

This function has two minima, one at displacement zero caused by the noise, and the other one at displacement $\boldsymbol{d}_k^o$ that has to be identified. For this purpose, we require the global minimum of $J_{2k}(\boldsymbol{d})$ to be located at $\boldsymbol{d} = \boldsymbol{d}_k^o$ and not at $\boldsymbol{d} = \boldsymbol{0}$, hence, $J_2(\boldsymbol{d}_k^o) < J_2(\boldsymbol{0})$. This inequality is expressed as a function of the noise and signal parameters as:

$$2\sigma_n^2 - 2\sigma_n^2 a_m^{|d_{km}^o|}\, a_n^{|d_{kn}^o|} a_k \;<\; 2\sigma_f^2 + 2\sigma_n^2 - 2\sigma_n^2\, a_k$$

$$\sigma_f^2 \;>\; \sigma_n^2 a_k - \sigma_n^2 a_m^{|d_{km}^o|}\, a_n^{|d_{kn}^o|} a_k .$$

This condition is equivalent to:

$$\sigma_f^2 > \sigma_n^2\, a_k\,(1- a_m^{|d_{km}^o|}\, a_n^{|d_{kn}^o|}). \tag{4.12}$$

Since $SNR = 10\log(\frac{\sigma_f^2}{\sigma_n^2})$, Eq. (4.12) becomes:

$$SNR > 10\log(a_k\,(1- a_m^{|d_{km}^o|}\, a_n^{|d_{kn}^o|})). \tag{4.13}$$

Consequently, this condition limits the *SNR*. There is not such a restriction for white noise, since it is only necessary that $(a_m=a_n=a_k=0)$,

$$\sigma_f^2 > 0$$

which is always true. Figure 4.1 shows $J_{2k}(d)$ for a uniform distributed 1-D white signal. Colored noise is generated as the output of a first-order AR system with coefficients $a_m=a_k=0.8$, which input is a white Gaussian distributed signal. The signal under analysis undergoes a displacement of $d_k^o = 8$, and the $SNR = 0\ dB$. For these parameter values, we obtain a theoretical absolute minimum at the desired displacement up to $SNR \approx -\ 1.7dB$. For lower SNR the absolute minimum is located at displacement zero and a local minimum is located at the correct displacement that tends to disappear when decreasing the SNR.

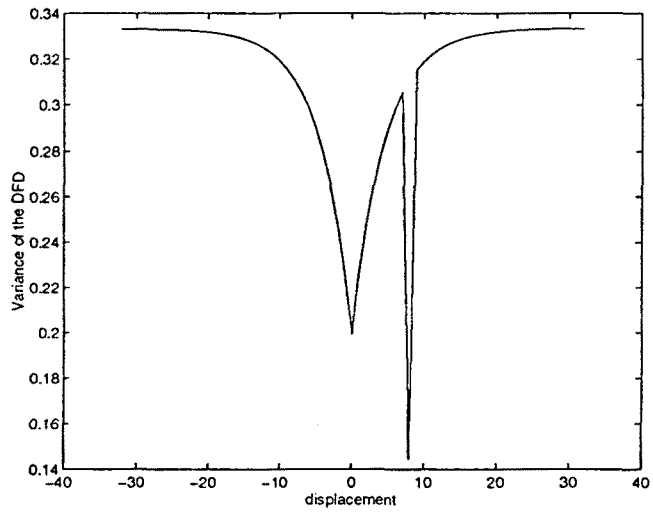

Fig 4.1 $J_{2k}(d)$ for an uncorrelated signal which AR noise coefficients are $a_m = a_k = 0.8$, and for $SNR = 0\ dB$.

4.2.2 Study for Correlated Region and Colored Noise

The effects of noise are even more harmful when there is correlation among pixels within a region or block. Considering this is a more likely situation, an analogous expression of the cost function must be derived. We model the signal as a stationary AR process and thus, the covariance within the region is given by [Jain]:

$$r_f(d) = \sigma_f^2 b_m^{|d_m|} b_n^{|d_n|}$$

where b_m and b_n are the spatial coefficients of the signal covariance. The cost function in this case becomes :

$$J_{2k}(d)=2\sigma_f^2-2\sigma_f^2 b_m^{|d_m-d_{km}^o|} b_n^{|d_n-d_{kn}^o|}+2\sigma_n^2-2\sigma_n^2 a_m^{|d_m|} a_n^{|d_n|} a_k \qquad (4.14)$$

As before, to obtain the correct displacement we require the global minimum of the function to be located at the desired displacement. The inequality $J_{2k}(d_k^o) < J_{2k}(0)$, is derived as a function of region and noise parameters:

$$2\sigma_n^2 - 2\sigma_n^2 a_m^{|d_{km}^o|} a_n^{|d_{kn}^o|} a_k \; < \; 2\sigma_f^2-2\sigma_f^2 b_m^{|-d_{km}^o|} b_n^{|-d_{kn}^o|})+2\sigma_n^2-2\sigma_n^2 a_k,$$

$$\sigma_f^2 - \sigma_f^2 b_m^{|d_{km}^o|} b_n^{|d_{kn}^o|} > \; \sigma_n^2 \; a_k \,(1- a_m^{|d_{km}^o|} a_n^{|d_{kn}^o|}),$$

$$\sigma_f^2 \; > \; \sigma_n^2 \, a_k \; \frac{1- a_m^{|d_{km}^o|} a_n^{|d_{kn}^o|}}{1- b_m^{|d_{km}^o|} b_n^{|d_{kn}^o|}},$$

and therefore the *SNR* should be at least:

$$SNR \; > \; 10\log(a_k \; \frac{1- a_m^{|d_{km}^o|} a_n^{|d_{kn}^o|}}{1- b_m^{|d_{km}^o|} b_n^{|d_{kn}^o|}}). \qquad (4.15)$$

Figure 4.2 shows $J_{2k}(d)$ for a 1-D first-order AR-modeled signal that is generated as the output of a system with coefficient $b_m = 0.8$, and which input is a white uniform distributed signal. The variance of the signal is related to the variance of the generating signal, x, as (Appendix C), $\sigma_x^2 = \sigma_f^2 - b_m^2 \sigma_f^2$. Likewise the AR noise coefficients are $a_m = a_k = 0.8$ and the $SNR = 0$ *dB*. The signal is displaced $d_k^o = 8$. For these parameters, we obtain an absolute minimum at the desired displacement up to $SNR \approx -1$ *dB*.

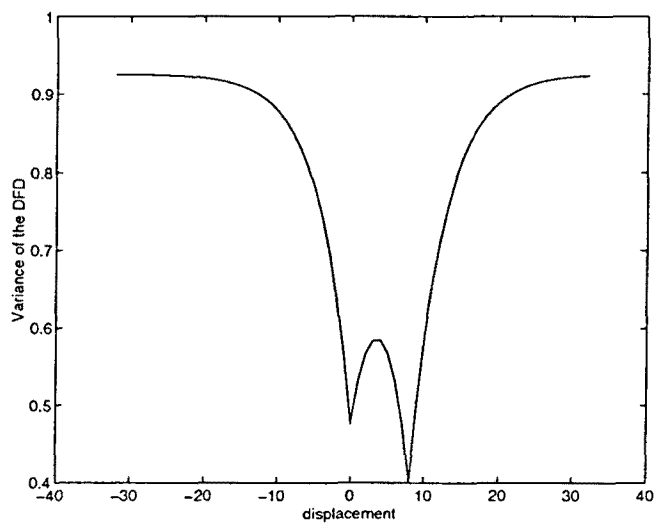

Fig 4.2 $J_{2k}(d)$ for a correlated signal which AR noise coefficients are $a_m = a_k = 0.8$ and AR signal coefficient is $b_m = 0.8$, $SNR = 0$ *dB*.

In figures 4.3 and 4.4 the SNR bounds are plot according to Eq. (4.12) and Eq. (4.15) to obtain the displacement from the absolute minimum of $J_{2k}(d)$. The displacement is fixed to d_k^o= *(0.5, 0.5)* in fig. 4.3 and d_k^o= *(8, 8)* in figure 4.4. It is interesting to observe that for a given displacement the SNR curve shows a maximum for some specific AR coefficients of the noise. The limit SNR is higher for correlated signals when the displacement is small (fig. 4.3) whereas this difference is not observed when the correct displacement is large (fig. 4.4). On the other hand, setting the AR coefficients and varying the optimum displacement the results show quite different behavior for white signals than for correlated signals (fig. 4.5). It is more easily seen here that for large displacement the SNR bounds tend to be the same for white and colored signals.

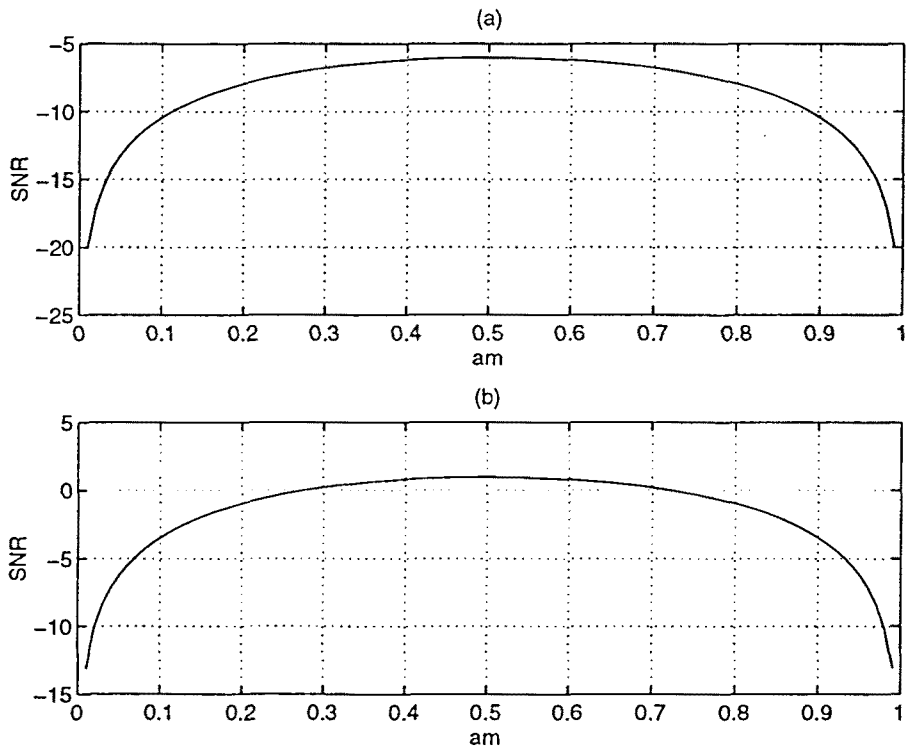

Fig 4.3 Minimum SNR curve for $J_{2k}(d_k^o)$ as a function of the noise AR parameters $a_n = a_m = a_k$ given d_k^o= *(0.5, 0.5)* a) for white signals b) for correlated signals *(b_m=b_n=0.8)*

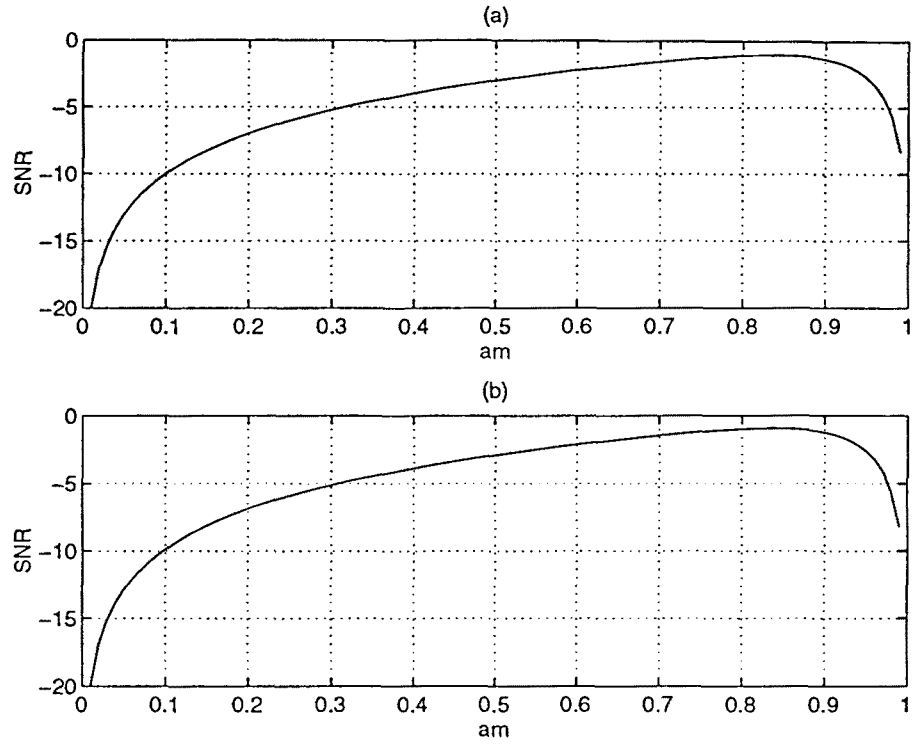

Fig 4.4 Minimum SNR curve for $J_{2k}(d_k^o)$ as a function of the noise AR parameters $a_n = a_m = a_k$ given $d_k^o = (8, 8)$ a) for white signals b) for correlated signals $(b_m = b_n = 0.8)$

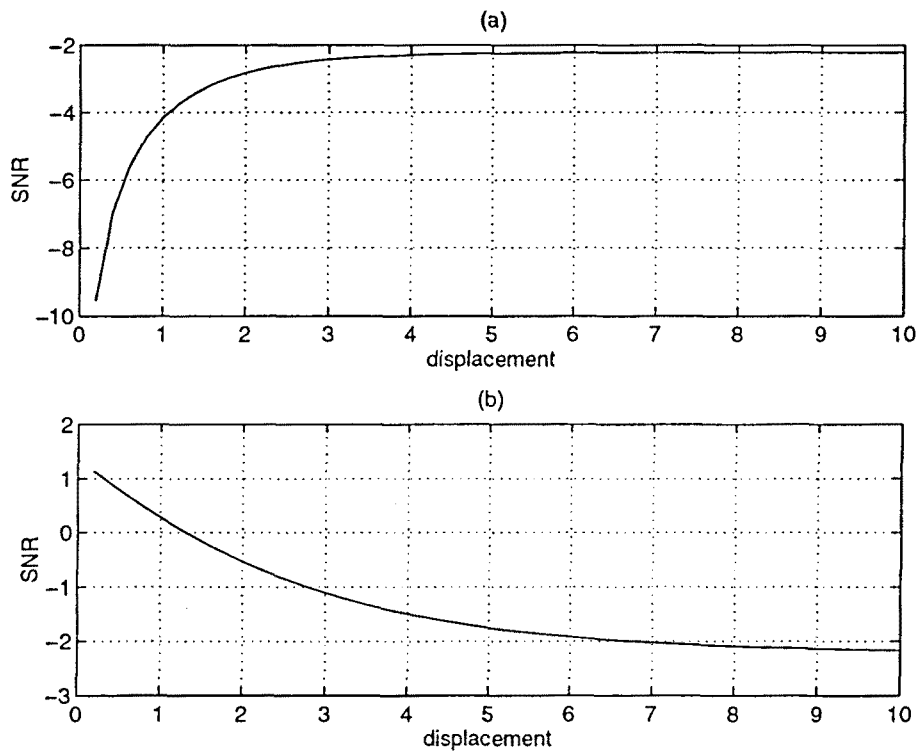

Fig 4.5 Minimum SNR curve for $J_{2k}(d)$ where $d_{km}^{\ o} = d_{kn}^{\ o}$. The noise AR parameters are fixed to $a_n = a_m = a_k = 0.6$, a) for white signals b) for correlated signals $(b_m = b_n = 0.8)$

4.3 Kurtosis of the DFD

We are interested in choosing a cost function based on HOS to reduce the effect of colored Gaussian noise. Recall from Chapter 2 that HOS methods are blind to Gaussian processes and thus, information due to deviations from Gaussianity may be extracted. Theoretically, this property will permit to detect the correct displacement for any SNR. This kind of cost functions can be built from different criteria. For example, the displacement can be found by maximizing or minimizing a function of moments, cumulants, or cross-cumulants. The approach in [Kleihorst, 1993] minimizes the third-order moment:

$$E\{g_{k-1}(m-d)\, g_k(m) g_{k+1}(m+d)\}$$

Another criterion is to apply cumulant or moment matching of regions. In [Anderson, 1991] a third-order cumulant matching criterion is proposed where the correct displacement is found by minimizing:

$$\sum\sum [C_{g_{k-1} g_k g_{k+1}}(\tau_1, \tau_2) - C_{g_{k-1} g_{k-1} g_{k-1}}(\tau_1 - d, \tau_2)]^2$$

The above third-order statistics cost functions reduce the effect of Gaussian noise, however they restrict the regions to be non-symmetrically distributed. As we saw in Chapter 2 odd-order cumulants of symmetrically distributed signals are zero and therefore are not appropriate to use. A third option consist on choosing a criteria based on a HOS-function of the displaced frame difference. The approach in [Anderson, 1994] is based on a fourth-order statistics cost function that utilizes the kurtosis of the $DFD_k(d)$, which is asymptotically unaffected by correlated Gaussian noise. It is defined as :

$$K(DFD_k(d)) = E\{DFD_k^4(d)\} - 3[E\{DFD_k^2(d)\}]^2 \qquad (4.15)$$

From the independence property of cumulants (property [P4] in Chapter 2), we obtain

$$K(DFD_k(d)) = K(DSD_k(d)) + K(DND_k(d))$$

If the noise is Gaussian or the kurtosis of its distribution is zero, even if it is colored, $K(DND_k(d)) = 0$, i. e., the kurtosis of the $DFD_k(d)$ only depends on the kurtosis of the $DSD_k(d)$. Therefore a suitable cost function is:

$$J_{41k}(d) = K(DFD_k(d)) \qquad (4.16)$$

$$\hat{d}_k^o \leftarrow \begin{matrix} min \\ max \end{matrix} (J_{41k}(d))$$

This cost function changes its sign depending on the kurtosis sign of the region. The correct displacement is found by minimizing $J_{41k}(d)$ when the region has a positive kurtosis or maximizing it when the kurtosis is negative. Tugnait [1989] was the first to propose this criterion to estimate the time delay between two signals as an extension to the performance index $J_{2k}(d)$. Latter, Anderson & Giannakis [1993] used the above cost function to recursively estimate the displacement of pixels between two images.

Consistent estimates of cumulants are those which are asymptotically unbiased and the variance tends to zero when $N \rightarrow \infty$ [Rosenblatt]. The corresponding consistent estimation of $J_{41k}(d)$ is given by:

$$\hat{J}_{41k}(d) = \frac{1}{N} \sum_{m \varepsilon \Omega_m} DFD_k^4(d) - 3 \left[\frac{1}{N} \sum_{m \varepsilon \Omega_m} DFD_k^2(d) \right]^2 \tag{4.17}$$

Asymptotically, the presence of noise does not degrade the detection process and the *shape* of the cost function will depend only on the statistics of the signal. We will now develop the theoretical kurtosis as a function of signal second and higher-order moments, latter some examples for finite regions will show that the estimation is, in practice, affected by the noise, since the estimation has a high noise-dependent variance.

As just mentioned, the kurtosis of the DFD depends only on the kurtosis of the displaced signal difference when noise is Gaussian distributed, thus for zero-mean processes:

$$J_{41k}(d) = K(DSD_k(d)) = E\{DSD_k^4(d)\} - 3E^2\{DSD_k^2(d)\}. \tag{4.18}$$

The two expectation terms are developed as a function of signal moments. We analyze first the term $E\{DSD_k^4(d)\}$ obtaining:

$$E\{DSD_k^4(d)\} = E\{(f_k(m) - f_{k-1}(m-d))^4\} =$$

$$E\{f_k^4(m)\} + E\{f_{k-1}^4(m-d)\} + 6E\{f_k^2(m) f_{k-1}^2(m-d)\}$$

$$- 4E\{f_k^3(m) f_{k-1}(m-d)\} - 4E\{f_k(m) f_{k-1}^3(m-d)\},$$

which can be further developed as a function of f_k only using Eq. (4.7). Thus, denoting the signal fourth-order moment as $m_{f4} = E\{ (f_k^4(m) \} = E\{ (f_k^4(m+d_k^o-d) \}$ we get:

$$E\{DSD_k^4(d)\} = 2m_{f4} + 6E\{f_k^2(m) f_k^2(m+d_k^o-d)\}$$

$$- 4E\{f_k^3(m) f_k(m+d_k^o-d)\} - 4E\{f_k(m) f_k^3(m+d_k^o-d)\} \tag{4.19}$$

Analogously, the second term in Eq. (4.18) can be derived as

$$E^2\{DFD_k^2(d)\} = (2\sigma_f^2 - 2r_f(d_k^o-d))^2 = 4\sigma_f^4 + 4r_f^2(d_k^o-d) - 8\sigma_f^2 r_f(d_k^o-d) \quad (4.20)$$

From Eq. (4.19) and Eq. (4.20) the cost function based on the kurtosis can be written in terms of the signal moments as :

$$\begin{aligned} J_{4Ik}(d) = {} & 2m_{f4} + 6E\{f_k^2(m)f_k^2(m+d_k^o-d)\} \\ & - 4E\{f_k(m)f_k^3(m+d_k^o-d)\} - 4E\{f_k^3(m)f_k(m+d_k^o-d)\} \\ & - 12\sigma_f^4 - 12r_f^2(d_k^o-d) + 24\sigma_f^2 r_f(d_k^o-d) \end{aligned} \quad (4.21)$$

This is the general expression for the kurtosis based cost function . Following the theoretical expressions considering uncorrelation and correlation among pixels are derived.

4.3.1. Study for Uncorrelated Region

For this cost function, we do not need to characterize colored Gaussian noise as we did in section 4.2.1 since noise terms vanish thanks to the independence property of cumulants. On the other hand, not only second-order but higher-order moments of the signal appear, as we see in Eq. (4.21). For the case of an uncorrelated signal these moments are the following:

$$E\{(f_k^2(m)\, f_{k-1}^2(m-d))\} = \sigma_f^4 + (m_{f4} - \sigma_f^4)\,\delta(d-d_k^o) \quad (4.22)$$

$$E\{(f_k(m)\, f_{k-1}^3(m-d))\} = E\{(f_k^3(m)\, f_{k-1}(m-d))\} = m_{f4}\,\delta(d-d_k^o) \quad (4.23)$$

Note that Eq. (4.22) is not zero for $d \neq d_k^o$. The cost function is therefore :

$$J_{4Ik}(d) = 2m_{f4} + 6[\sigma_f^4 + (m_{f4} - \sigma_f^4)\delta(d-d_k^o)] - 8m_{f4}\,\delta(d-d_k^o) - 12\sigma_f^4 + 12\sigma_f^4\,\delta(d-d_k^o) \quad (4.24)$$

Figure 4.6 shows $J_{4Ik}(d)$ for a 1-D signal uniformly distributed that has negative kurtosis, which value is given by $m_{f4} - 3\sigma_f^4 = -18/15$, where $m_{f4} = 9/5$ and $\sigma_f^2 = 1$. The cost function has a negative constant value, except a unique maximum at $d_k^o = 8$ where the cost function is zero. For a positive kurtosis the constant value would be positive and the unique minimum, in this case, would be at the correct displacement. As we have pointed out, this result is maintained for any *SNR*.

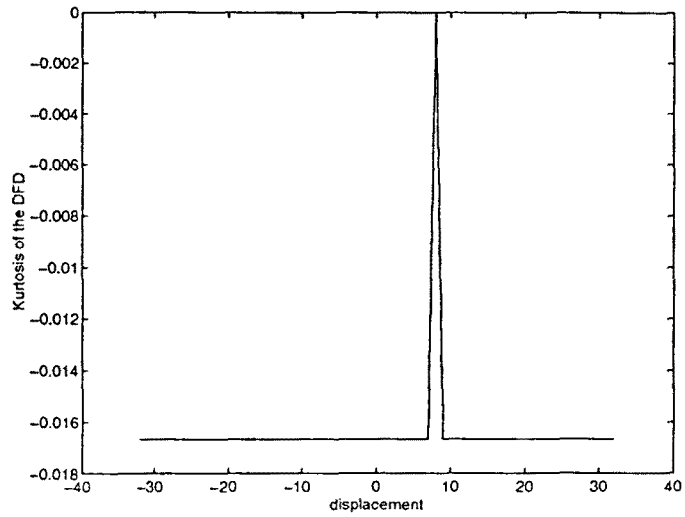

Fig 4.6 $J_{41k}(d)$ for an uncorrelated signal.

4.3.2. Study for Correlated Region

To study the behavior of $J_{41k}(d)$ for correlated signals, we consider a first-order AR model for 1-D signals. The reason to use 1-D signals is to avoid computing HOS components that are too cumbersome to derive for 2-D signals. The 1-D components are developed in Appendix C. It is proven there that:

$$E\{f_k^2(m) f_k^2(m-(d-d_k^o))\} = m_{f4}\,(b_m)^{2\,|d-d_k|} + \sigma_f^4 - (b_m)^{2|d-d_k|}\,\sigma_f^4 \tag{4.25}$$

The other higher-order terms are somewhat more difficult to obtain since they are different depending on the sign of $(d-d_k^o)$. We define (see Appendix C):

$$\Gamma_f(b_m,(d-d_k^o)) = (m_{f4} - 3\,\sigma_f^4)\,(b_m)^{3\,|d-d_k|} + 3(b_m)^{|d-d_k|}\,\sigma_f^4 \tag{4.26}$$

$$\Psi_f(b_m,d-d_k^o) = b_m^{|d-d_k|} m_{f4} \tag{4.27}$$

It is shown that

$$E\{(f_k^3(m)\, f_k(m-(d-d_k^o)))\} = \begin{cases} \Gamma_f(b_m,d-d_k^o) & (d-d_k^o)>0 \\ \Psi_f(b_m,d-d_k^o) & (d-d_k^o)<0 \end{cases} \tag{4.28}$$

and

$$E\{f_k(m)f_{k-1}^3(m-(d-d_k^o))\}=\begin{cases}\Psi(b_m,d-d_k^o) & (d-d_k^o)>0\\ \Gamma f(b_m,d-d_k^o) & (d-d_k^o)<0\end{cases} \quad (4.29)$$

Thus,

$$J_{41k}(d) = 2m_{f4}+6\,[m_{f4}(b_m)^{2\,|d-d_k|} + \sigma_f^4 - (b_m)^{2|d-d_k|}\,\sigma_f^4]$$

$$- 4\Psi f(b_m,d-d_k^o) - 4\,\Gamma f(b_m,d-d_k^o) - 12\sigma_f^4 - 12\sigma_f^4 b_m^{2|d-d_k^o|} + 24\,\sigma_f^4 b_m^{|d-d_k^o|} \quad (4.30)$$

Figure 4.7 shows $J_{41k}(d)$ for a 1-D AR-modeled signal that is generated as the output of a system with coefficients $b_m = 0.8$, which input is a white uniformly distributed signal. The kurtosis of the signal is related to the input generating signal, x, as (Appendix C), $(m_{f4} - 3\,\sigma_f^4) = (m_{x4} - 3\,\sigma_x^4)/(1-b_m^4)$. For a correlated signal the peak has broaden at the desired extremum at $d_k^o = 8$.

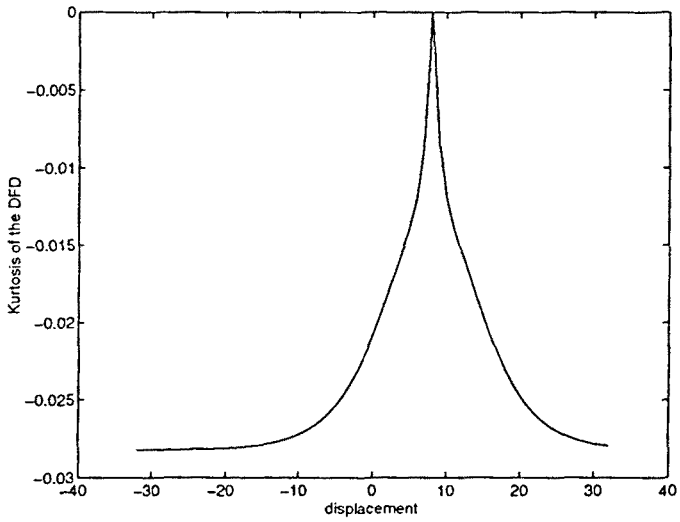

Fig 4.7 $J_{41k}(d)$ for correlated signal.

We have just obtained the statistical mean estimates of the second-order and fourth-order-based cost functions. Independently of low or high correlation among the pixels of the noise-free regions, $J_{2k}(d)$ is degraded by the presence of colored Gaussian noise. On the other hand, the mean estimation of $J_{41k}(d)$ is not affected by this type of noise.

As important as the mean of the estimation is the variance of the estimation. The following examples are given to compare the variance when estimating $J_{2k}(d)$ and $J_{41k}(d)$. For this purpose, we generate several times 1-D signals and each time we estimate the cost functions as they are defined in Eq. (4.5) and (4.17). At last we compute the mean estimation of the cost functions and their variances.

Example 4.1 : We determine $J_{2k}(d)$ and $J_{41k}(d)$ for a rectangular 1-D object of length 256 which kurtosis is negative. We use 20 different realizations to study the mean and variance of these indexes. In first place, we observe their behavior for moderate SNR. Thus, fig. (4.8a) and (4.8b) show the estimation for $SNR = 15\ dB$, the pixels of the signal are uncorrelated and the Gaussian noise follows an AR model with $a_m = a_k = 0.8$. Each figure shows: in solid line, the mean of the cost function using 20 realizations of a sequence of two

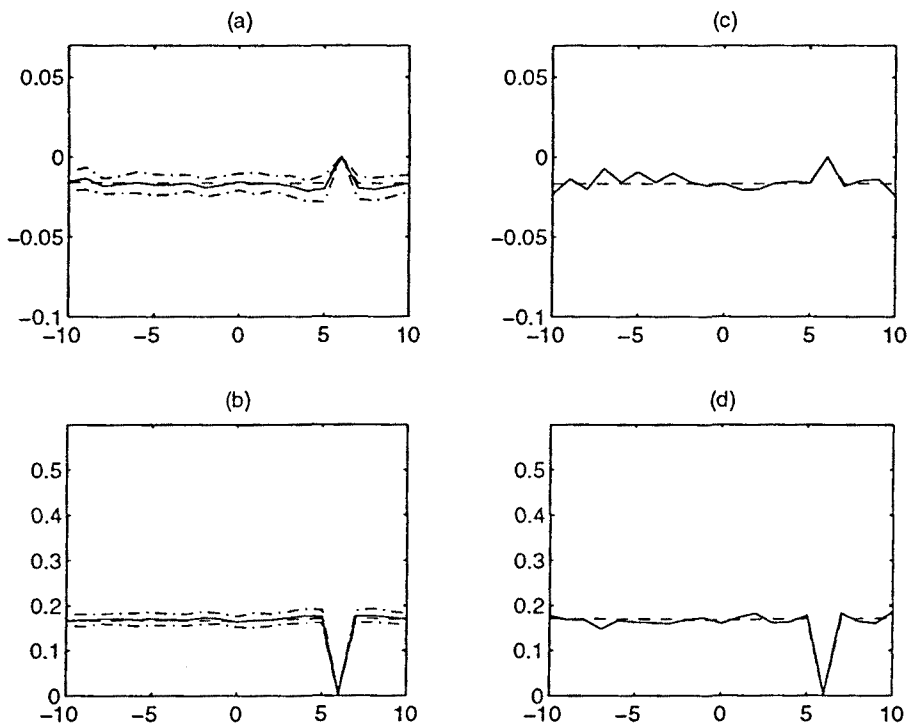

Fig 4.8 Cost functions for $SNR = 15\ dB$ of a 256 length object where $d_k^O = 6$; a) $J_{41k}(d)$ b)$J_{2k}(d)$ c) single realization of $J_{41k}(d)$ and d) single realization of $J_{2k}(d)$

signals, where $d_k^O = 6$; in dashed line, the theoretical cost function; and finally, in dashed-dot line, the mean plus/minus the standard deviation. Figures (4.8c) and (4.8d) show the

estimation for a single realization. The mean estimation is close to the theoretical expectations. The kurtosis-based measure seems to have a higher variance. This fact can be confirmed for lower SNR. Figures (4.9a) and (4.9b) show the mean estimation for both cost functions as well as the mean plus/minus standard deviation when *SNR = -2.5 dB* (this SNR was chosen since it is close to the theoretical limit to obtain an absolute minimum using the second-order based index, which is -2.3 dB for these parameters). Clearly, although the mean estimation of the kurtosis tends to the theoretical result the variance is too high. Figure (4.9c) And (4.9d) show the estimation for a single realization. A better way to compare the variance is obtained normalizing both cost functions by their respective mean estimation. Thus, using the same scaling we appreciate in fig. (4.10a) and (4.10b) the normalized cost functions for low SNR (-2.5 dB) and in fig. (4.10c) and (4.10d) for high SNR (15 dB). These results suggest that the kurtosis-based cost function should not be used for low SNR unless dealing with longer signals which would reduce the variance. We must be aware of the fact that we are going to use this cost functions for image regions or blocks and the number of pixels may not be large.

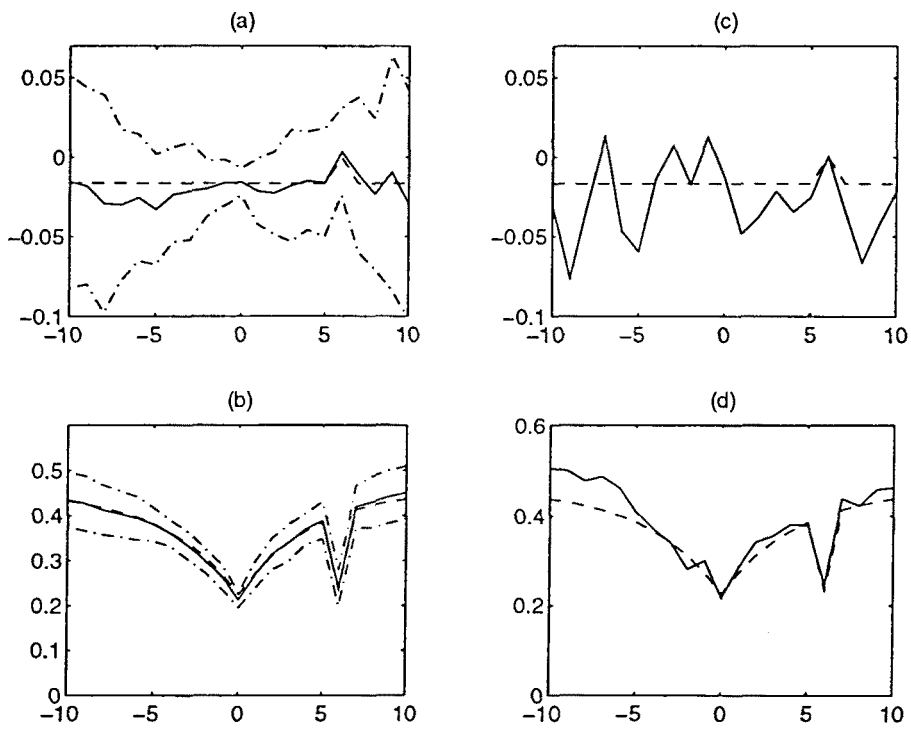

Fig 4.9 Cost functions for *SNR = -2.5 dB* of a 256 length object where $d_k^O=6$, a) $J_{41k}(d)$ b) $J_{2k}(d)$ c) single realization of $J_{41k}(d)$ and d) single realization of $J_{2k}(d)$

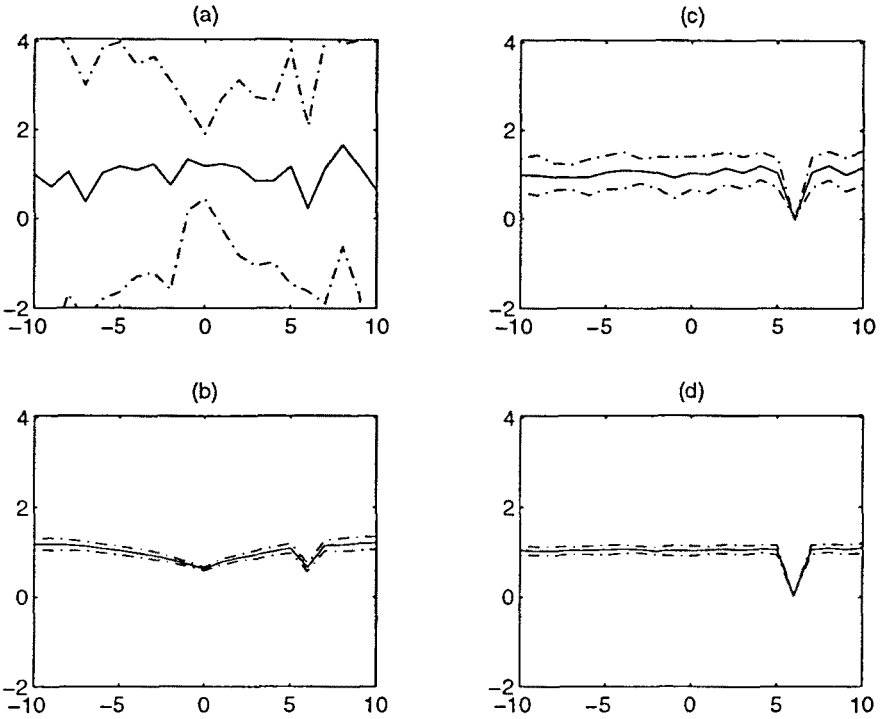

Fig 4.10 Normalized cost functions of a 256 length object where $d_k^o=6$, a) $J_{41k}(d)$ and b)$J_{2k}(d)$ for $SNR = -2.5\ dB$, c) $J_{41k}(d)$ and d)$J_{2k}(d)$ for $SNR = 15\ dB$

.4 Modified Kurtosis of the DFD

As we have shown in the previous section, the kurtosis is a very sensitive measure and we need long data records to obtain low variance estimates. On the other hand, image information is repeated along the sequence as it is established in the Intensity Constancy equation, Eq. (4.2). This redundancy may be used to obtain better estimates of the higher-order statistics to reduce the effect of additive noise. Amblard et al. [1993], proposed an adaptive scheme for the estimation of fourth-order cumulants for transient detection. It was proven for the case of i.i.d. random variables that the estimator is asymptotically unbiased. Using this approach, we derived the equivalent expression for the kurtosis of the displaced frame difference which at time k becomes:

$$\hat{K}_k(DFD(d))) = \hat{K}_{k-1}(DFD(d)) + \gamma[\hat{k}(DFD_k(d)) - \hat{K}_{k-1}(DFD(d))], \qquad (4.31)$$

where $\hat{k}(DFD_k(d)))$ is the "instantaneous kurtosis" given by,

$$\hat{k}(DFD_k(d)) = \frac{1}{N}\sum_{m\varepsilon\Omega_m} DFD_k^4(d) - 3[\frac{1}{N}\sum_{m\varepsilon\Omega_m} DFD_k^2(d)\,\hat{E}_{k-1}\{DFD^2(d))], \quad (4.32)$$

and

$$\hat{E}_k\{DFD^2(d)) = \hat{E}_{k-1}\{DFD^2(d)\} + \mu\,[\frac{1}{N}\sum_{m\varepsilon\Omega_m} DFD_k^2(d) - \hat{E}_{k-1}\{DFD^2(d))], \quad (4.33)$$

μ and γ are forgetting factors that adapt the estimation to changing conditions. The sub index k has been suppressed in the *DFDs* where previous frames are involved. This adaptive scheme leads to consistent estimates of the kurtosis of the DFD.

Nevertheless, we are interested in obtaining the displacement vector at time k and this only depends on the instantaneous kurtosis, that is, Eq. (4.32) and (4.33). It is clear that there is no information on the current displacement between two frames in previous images or in previous displacements (unless we were dealing with some kind of prediction or motion model). Previous frames can be used to obtain information on the statistics of the regions and/or statistics of the noise. Our goal is to define a low variance cost function which should be, at the same time, asymptotically unaffected by correlated Gaussian noise. One possible solution is based on the instantaneous kurtosis defined by Eq. (4.32), which is normalized to the square of the variance:

$$\hat{J}_{42k}(d) = \frac{1}{\hat{J}_{2k}^2(d)} \cdot [\frac{1}{N}\sum_{m\varepsilon\Omega_m} DFD_k^4(d) - 3\,\frac{1}{N}\sum_{m\varepsilon\Omega_m} DFD_k^2(d)\,\hat{E}_{k-1}\{DFD^2(d))\,] \quad (4.34)$$

For $\mu = 1$ only the previous DFD intervenes, and therefore, only three frames are included:

$$\hat{J}_{42k}(d) = \frac{1}{\hat{J}_{2k}^2(d)} \cdot \frac{1}{N}\sum_{m\varepsilon\Omega_m} DFD_k^4(d) - 3\,\frac{1}{N}\sum_{m\varepsilon\Omega_m} DFD_{k-1}^2(d)\,\frac{1}{N}\sum_{m\varepsilon\Omega_m} DFD_k^2(d) \quad (4.35)$$

For small values of μ past frames become more significant than the previous one. Thus, depending on the estimation of $\hat{E}_{k-1}\{DFD^2(d))$, different versions of the above cost function may be derived. Observe that instead of having the instantaneous second-order moment estimate to the power of two, which may show a high variance, we have a term whihc is the product of the instantaneous second-order moment by the estimated second-order moment using more than two frames.

In terms of expectations Eq. (4.34) is rewritten as:

$$J_{42k}(d) = \frac{1}{[E\{DFD_k^2(d)\}]^2} \cdot E\{DFD_k^4(d)\} - 3\,E\{DFD_k^2(d)\}\;E_{k-1}\{DFD^2(d)\}. \quad (4.36)$$

An alternative estimation is necessary in case only two frames are available or when the first two frames of a sequence are not static. In this case, it seems reasonable to use the kurtosis cost function as it is defined in Eq. (4.17) and normalize by the square of the variance. Another approach that we propose using Eq. (4.34) with:

$$E_{k-1}(DFD^2(d)) \longrightarrow \frac{1}{N} \sum_{m \varepsilon \Omega_m} [g_{k-1}(m) - g_{k-1}(m-d)]^2, \tag{4.37}$$

is given by:

$$\hat{J}_{43k}(d) = \frac{1}{\hat{J}_{2k}^2(d)} \left[\frac{1}{N} \sum_{m \varepsilon \Omega_m} DFD_k^4(d) - 3 \frac{1}{N} \sum_{m \varepsilon \Omega_m} [g_{k-1}(m) - g_{k-1}(m-d)]^2 \frac{1}{N} \sum_{m \varepsilon \Omega_m} DFD_k^2(d) \right]. \tag{4.38}$$

The resulting cost function will display a behavior similar to the one in Eq. (4.35), yielding to better estimates of the displacement.

To study these cost functions we derived also the moments of the *DFD* as a function of signal and noise moments. The development is shown in Appendix D for $J_{42k}(d)$, when $\mu=1$, and for $J_{43k}(d)$, where we substitute the summation by the expectation operator. The results are illustrated in the following sections.

The first step is to decompose $J_{42k}(d)$ in signal and noise differences. Thus, we obtain their contributions (Appendix D):

$$J_{42k}(d) = \frac{1}{J_{2k}^2(d)} \{ E\{DSD_k^4(d)\} - 3E\{DSD_k^2(d)\}E\{DSD_{k-1}^2(d)\}$$

$$-3E\{DND_k^2(d)\}[E\{DSD_{k-1}^2(d)\} - E\{DSD_k^2(d)\}] \} \tag{4.39}$$

which for $\mu=1$ leads to the expression (Appendix D):

$$J_{42k}(d) = \frac{1}{J_{2k}^2(d)} \{$$

$$2m_{f4} + 6E\{f_k^2(m) f_k^2(m+d_k^o-d)\} - 4E\{f_k^3(m) f_k(m+d_k^o-d)\} - 4E\{f_k(m) f_k^3(m+d_k^o-d)\}$$

$$- 3[2\sigma_f^2 - 2r_f(d_k^o-d)] [2\sigma_f^2 - 2r_f(d_{k-1}^o-d)]$$

$$-3[2\sigma_n^2 - 2r_{n1}(d)] [2r_f(d_k^o-d)] - 2r_f(d_{k-1}^o-d)\} \tag{4.40}$$

This is the general expression of the new-defined cost function as a function of the signal and noise moments. Analogously as we did for the previous cost functions, analytical expressions may be derived for the case of correlated and uncorrelated signals.

4.4.1 Study for Uncorrelated Region and Colored Noise:

In this case we obtain:

$$J_{42k}(d) = \begin{cases} \dfrac{2m_{f4}-6\sigma_f^4}{[2\sigma_f^2+2\sigma_n^2(1-a_m^{|d_m|}a_n^{|d_n|}a_k)]^2} & d\neq d_k^o\neq d_{k-1}^o \\ \dfrac{-6\sigma_f^2}{2\sigma_n^2(1-a_m^{|d_k^o|}a_n^{|d_k^o|}a_k)} & d=d_k^o \\ \dfrac{2m_{f4}-6\sigma_f^4+12\sigma_f^2\sigma_n^2[1-a_m^{|d_{k-1}^o|}a_n^{|d_{k-1}^o|}a_k]}{[2\sigma_f^2+2\sigma_n^2(1-a_m^{|d_{k-1}^o|}a_n^{|d_{k-1}^o|}a_k)]^2} & d=d_{k-1}^o \end{cases}$$

Although noise is affecting the behavior of the cost function it does in an appropriate manner. The cost function is characterized in three different areas. In the first one, when the displacement variable is different from the correct current and previous displacements, we obtain the normalized kurtosis which sign depends on the sign of the region kurtosis. When the variable is equal to the current displacement, the value of the cost function is negative. Finally, for the previous displacement, we obtain a value which is higher than the normalized kurtosis. Thus the usual shape of the cost function will show a maximum at the previous displacement and a minimum at the correct displacement. This will be better seen in the examples.

4.4.2 Study for Correlated Region and Colored Noise:

The analytical expression for the case of 1-D correlated signals is the following:

$$J_{42k}(d) = \frac{1}{2\sigma_f^2+2\sigma_n^2(1-a_m^{|d_m|}a_n^{|d_n|}a_k)]^2}\{$$

$$2m_{f4}+6[m_{f4}(b_m)^{2|d-d_k|}+\sigma_f^4-(b_m)^{2|d-d_k|}\sigma_f^4]-4\Psi_f(b_m,d-d_k^o)-4\Gamma_f(b_m,d-d_k^o)$$

$$-12\sigma_f^4[1-b_m^{|d-d_k^o|}][1-b_m^{|d-d_{k-1}^o|}]$$

$$-12\sigma_n^2\sigma_f^2[1-a_m^{|d_m|}a_n^{|d_n|}a_k)][b_m^{|d-d_k^o|}-b_m^{|d-d_{k-1}^o|}]\}$$

where the moment functions were obtained in Sections 4.2 and 4.3 for AR models. It is not obvious to recognize what is the behavior of $J_{42k}(d)$ for different displacements. From Eq. (4.40) we can notice that there is a noise term that multiplies a difference of displaced signal covariances. Thus, if the optimal displacements at time k and $k-1$ are equal, we can easily deduce that $J_{42k}(d)$ is nothing else than the normalized kurtosis of the $DFD_k(d)$. For other situations, the following examples will clarify what is, in general, the behavior of this cost function.

Example 4.2 : We either assume the signal is uncorrelated or follows an AR model which input is an i.i.d. sequence uniformly distributed. We use the coefficients $a_m = a_k = 0.6$ for the noise and $b_m = 0.9$ for the signal, the *SNR* is set to *0 dB*. Figures (4.11a) and (4.11b) show $J_{42k}(d)$ for an uncorrelated and a correlated signal respectively. The displacement is $d_k^o = 8$ and $d_{k-1}^o = 0$. We observe that there is a minimum at the correct displacement and a maximum at displacement zero. As we pointed out, the noise is affecting $J_{42k}(d)$ in an advantageous manner. Figures (4.11c) and (4.11d) show the theoretical behavior of $J_{42k}(d)$ for an uncorrelated and a correlated signal respectively when $d_{k-1}^o = d_k^o$. For this case, the cost function behaves as the normalized kurtosis. It displays a maximum at the correct displacement when the region has negative kurtosis and a minimum when the region kurtosis is positive. The minimum we obtain at displacement zero is due to the normalization factor, the square variance estimate.

We also study the situation when the displacement changes slowly along the sequence. Figures (4.12a) and (4.12b) show $J_{42k}(d)$ when $d_k^o = 8$ and $d_{k-1}^o = 7$. As expected, we obtain a maximum at the previous displacement and a minimum at the current displacement. The same thing occurs when $d_k^o = 8$ and $d_{k-1}^o = 9$, see fig. (4.12c) and (4.12d). However we perceive a local minimum at displacement zero which is caused by the noise covariance. This could lead to incorrect results for other AR parameters and different SNR. Fortunately, we have observed that this only happens for extremely low SNR. For white signal this problem does not happen at all.

Figure (4.13) shows, for the same situation of d_k^o close to d_{k-1}^o, the behavior of the cost function when the signal has positive kurtosis. In this case we do not observe any local minimum at $d = 0$ even for extremely low SNR.

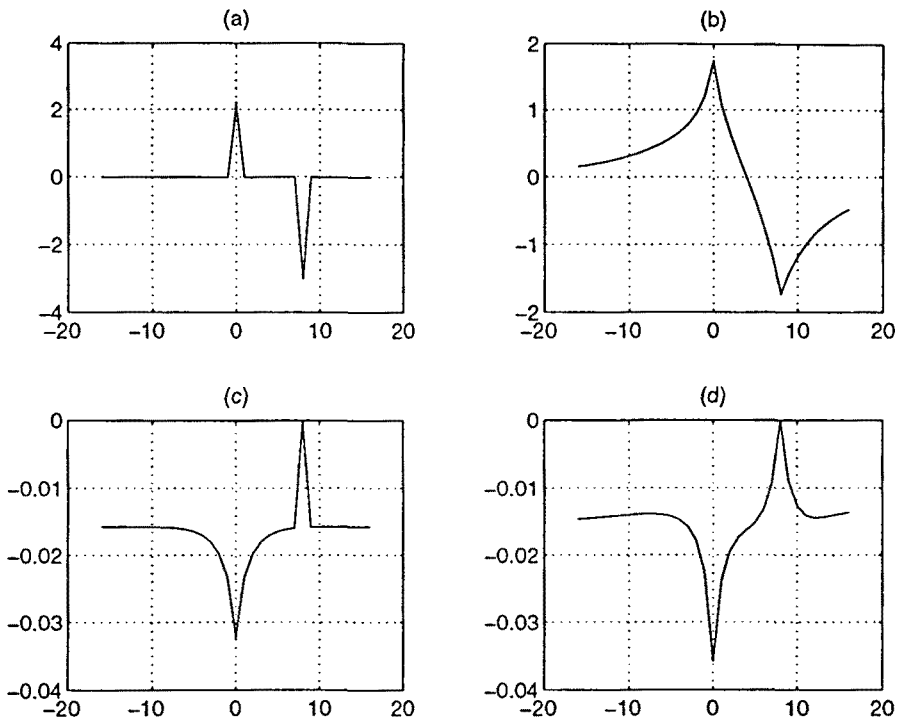

Fig 4.11 $J_{42k}(d)$ for a negative kurtosis region a) uncorrelated signal $d_k^o = 8$, $d_{k-1}^o = 0$, b) correlated signal, c) uncorrelated signal $d_k^o = d_{k-1}^o$, d) correlated signal.

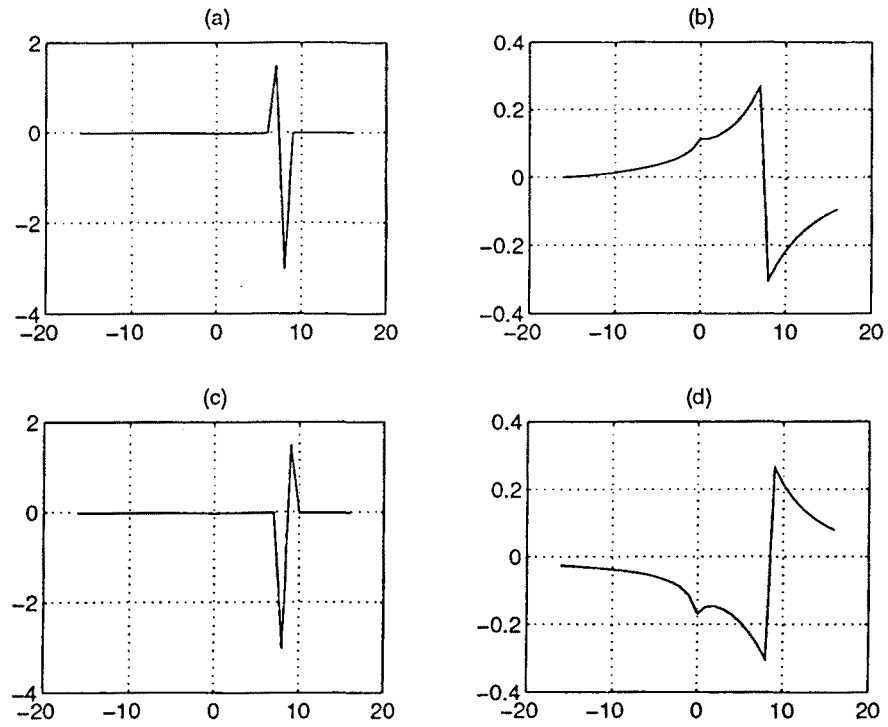

Fig 4.12 $J_{42k}(d)$ for a negative kurtosis region a) uncorrelated signal $d_k^o = 8$, $d_{k-1}^o = 7$, b) correlated signal, c) uncorrelated signal $d_k^o = 8$, $d_{k-1}^o = 9$, d) correlated signal.

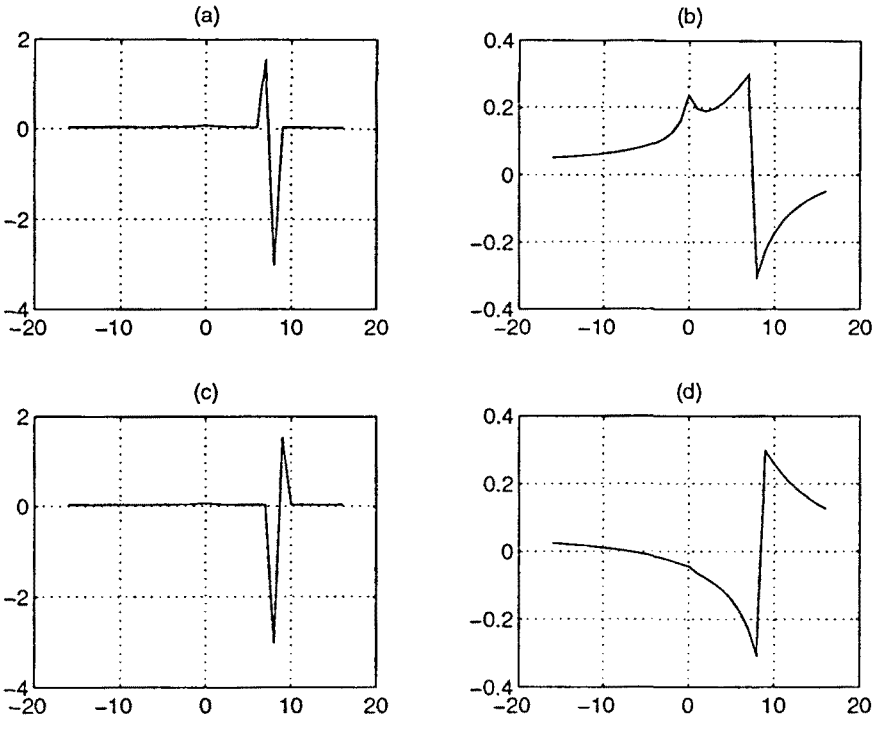

Fig 4.13 $J_{42k}(d)$ for a positive kurtosis region a) uncorrelated signal $d_k^o = 8$, $d_{k-1}^o = 7$, b) correlated signal, c) uncorrelated signal $d_k^o = 8$, $d_{k-1}^o = 9$, d) correlated signal.

We can then conclude that the new-defined cost function exhibits always an absolute minimum at the desired displacement for positive kurtosis regions. The same behavior is observed for negative kurtosis regions except when $d_{k-1}^o = d_k^o$, in which case the cost function becomes the normalized kurtosis. In this situation, the extremum at the desired displacement becomes a maximum. Hence, except for this case, in all other situations the correct displacement is derived from an absolute minimum. We need to introduce a mechanism to avoid searching a wrong minimum when $d_{k-1}^o = d_k^o$. One approach is to use $\mu<1$, thus, the influence of previous frames allows to keep a minimum at the desired displacement. If this situation stands for many frames we end up in the same situation. An additional step is added which consist of introducing a shift of $-d_{k-1}^o$ to $\hat{E}_{k-1}\{DFD^2(d)\}$. Thus, in the following iteration, $\hat{k}(DFD_k(d)))$ will have a maximum at $d=0$ and a minimum at $d=d_k^o$.

Next we present some examples where we compare the three cost functions defined up to this point. We will see the effects of the estimation and the advantages of using the newly defined cost function. We also test the above procedures for the case of $d_{k-1}^{o} = d_k^{o}$.

Example 4.3 : In this example we compare the performance indexes for a white 1-D rectangular object of length 256, which is moving along three frames where $d_{k-1}^{o} = 0$ and $d_k^{o} = 8$. Noise is simulated using an AR model with $a_m = a_k = 0.6$ and $SNR = -5\ dB$. As in example 4.1, we generate the sequence 20 times and obtain the mean behavior of the cost function at time k (we represent in dashed line the theoretical curve; in solid line the mean-estimation of the cost function; and in dashed-dot line the mean +/- the variance of the estimation) . We can observe in fig. 4.14b that the kurtosis cost function does not show the maximum at the correct displacement and exhibits high variance. We have normalized this cost function by $J_{2k}^{2}(d)$ to study if there is any improvement, which does not happen as it is illustrated in fig. 4.14a. Figure 4.14c shows $J_{42k}(d)$ using the estimation in Eq. (4.35), that is for $\mu = 1$, where only the previous displacement is relevant. For the modified kurtosis the variance is much lower and follows the theoretical results. Thus, this cost function can be reliably used for objects of this size in similar situations. For $J_{2k}(d)$ in fig. 4.14d the variance is low, but for this SNR the minimum at the correct displacement is not absolute. The limit SNR for these parameters is found to be $-2.29\ dB$ from a 1-D version of Eq. (4.13). Figure 4.15 shows the cost functions for a single sequence realization. The modified kurtosis cost function outperforms all other cost functions.

In the next step, we compare the cost functions for a highly correlated signal and find there is also an improvement in detecting motion using the new cost function. Figures 4.16 and 4.17 depict the mean behavior and a single realization of the cost functions for a 1-D colored rectangular signal following an AR model which parameter is $b_m = 0.8$. The SNR is $-2dB$ and the noise parameters are the same. The limit SNR in this case is -1.49 dB given from a 1-D version of Eq. (4.15). $J_{42k}(d)$ shows a minimum that is easily detected. $J_{2k}(d)$ shows two similar minima at the previous and current displacement.

Example 4.4 : In this example we compare $J_{42k}(d)$ and $J_{2k}(d)$ for a 2-D white uniformly distributed object of size 16x16. Colored noise that follows an AR model with $a_n = a_m = a_k = 0.8$ is added to a sequence of three images where the object is displaced $d_{k-1}^{o} = (0,0)$ and $d_k^{o} = (4,1)$. The SNR is set to $0\ dB$. The absolute minimum for $J_{2k}(d)$ corresponds to the displacement vector (0,0), whereas a relative minimum appears at (4,1) which is the correct displacement (fig. 4.18 and 4.19). On the other side, the absolute

minimum for $J_{42k}(d)$ is (4,1). We found that for this type of signal and $SNR = 0\ dB$ we obtain an 80% of error for $J_{2k}(d)$ versus 10% of error for $J_{42k}(d)$.

Example 4.5 : In this example we study the situation when the displacement changes slowly along the sequence. The signal and noise parameters are characterized by the same values than in Example 4.3 and the *SNR* is *-2 dB*. Figures (4.20a) shows a single realization of $J_{42k}(d)$ when $d_k^o = 8$, $d_{k-1}^o = 7$ and $d_{k-2}^o = 0$. As expected, we obtain a maximum at the previous displacement and a minimum at the current displacement. This situation is improved when $\mu = 0.89$ in the recursive estimation of $\hat{E}_{k-1}\{DFD^2(d))$ as it can be seen in fig. (4.20c). The same comments are valid for the case of $d_k^o = 8$, $d_{k-1}^o = 9$ and $d_{k-2}^o = 0$, see fig. (4.20b) and (4.20d).

Example 4.6 :We also compare the tracking capabilities with the ones of $J_{2k}(d)$ using the procedure to center $\hat{E}_{k-1}\{DFD^2(d))$ at d_{k-1}^o and using $\mu = 0.89$. We are given 10 realizations of a sequence of 7 synthetic noise free images containing an uncorrelated 2-D rectangular object. The object was previously segmented and was moving (3,1) pixels per frame. Colored Gaussian noise was generated from a first order AR model with $a_n = a_m = a_k = 0.6$ and added to the sequence. For this size and signal distribution, the cost function $J_{41k}(d)$ did not work at all. Table 1 shows the percentage errors to reach the final position for different sizes and SNR.

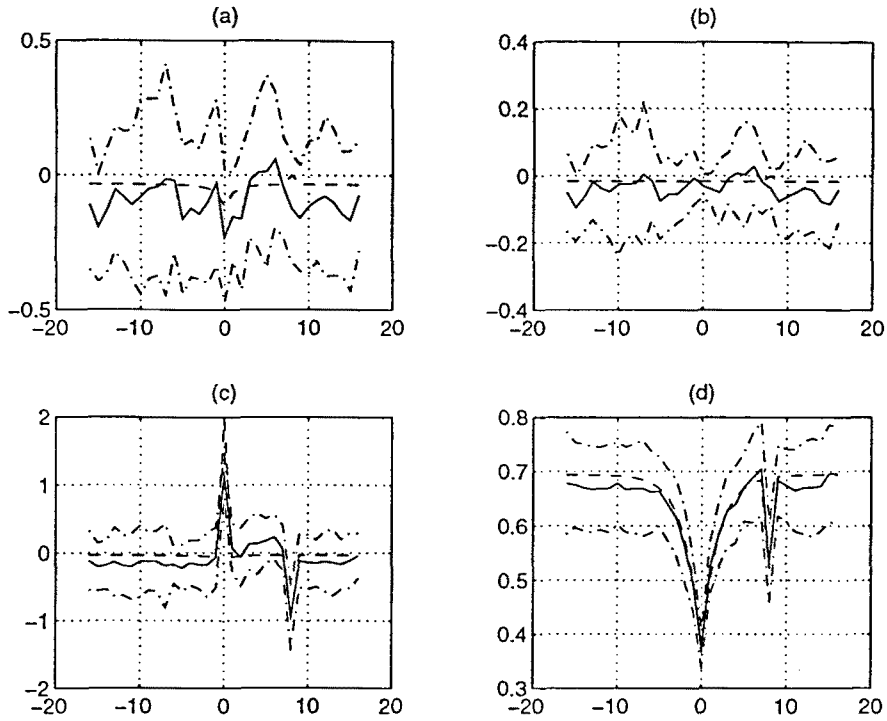

Fig 4.14 Estimated cost functions when $d_{k-1}^{o} = 0$, $d_k^{o} = 8$ *and SNR = -5 dB* for a white signal of length 256: a) $J_{41k}(d)$ normalized; b)$J_{41k}(d)$; c) $J_{42k}(d)$; d) $J_{2k}(d)$

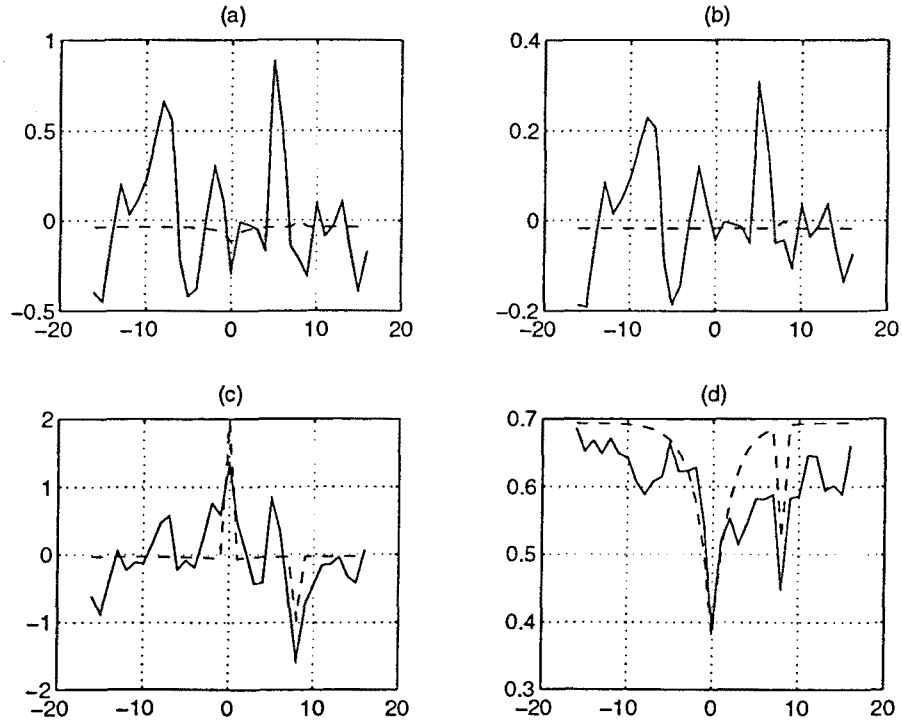

Fig 4.15 Cost functions for a single realization when $d_{k-1}^{o} = 0$, $d_k^{o} = 8$ *and SNR = -5 dB* for a white signal of length 256: a) $J_{41k}(d)$ normalized; b) $J_{41k}(d)$; c) $J_{42k}(d)$; d) $J_{2k}(d)$

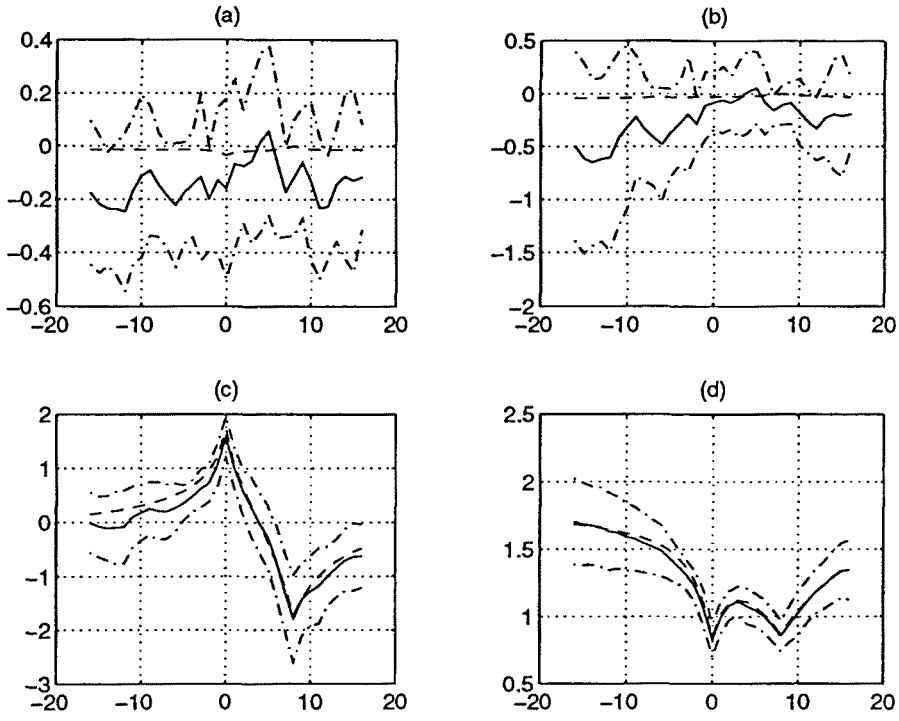

Fig 4.16 Estimated cost functions when $d_{k-1}^{o} = 0$, $d_k^{o} = 8$ *and SNR = -2 dB* for a colored signal of length 256: a) $J_{41k}(d)$ normalized; b) $J_{41k}(d)$; c) $J_{42k}(d)$; d) $J_{2k}(d)$

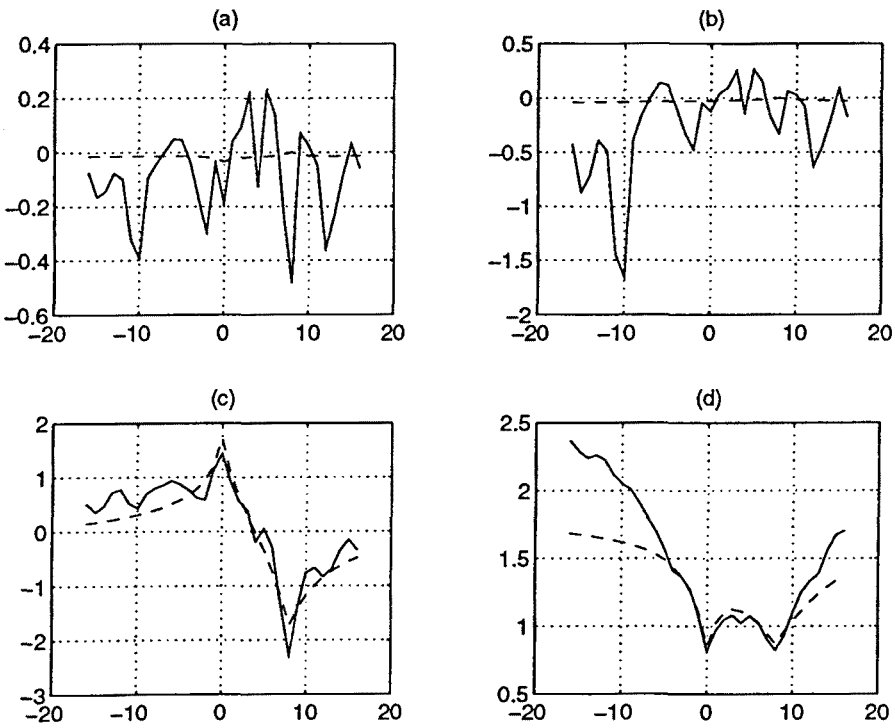

Fig 4.17 Cost functions for a single realization when $d_{k-1}^{o} = 0$, $d_k^{o} = 8$ *and SNR = -2 dB* for a colored signal of length 256: a) $J_{41k}(d)$ normalized;b)$J_{41k}(d)$; c) $J_{42k}(d)$; d)$J_{2k}(d)$

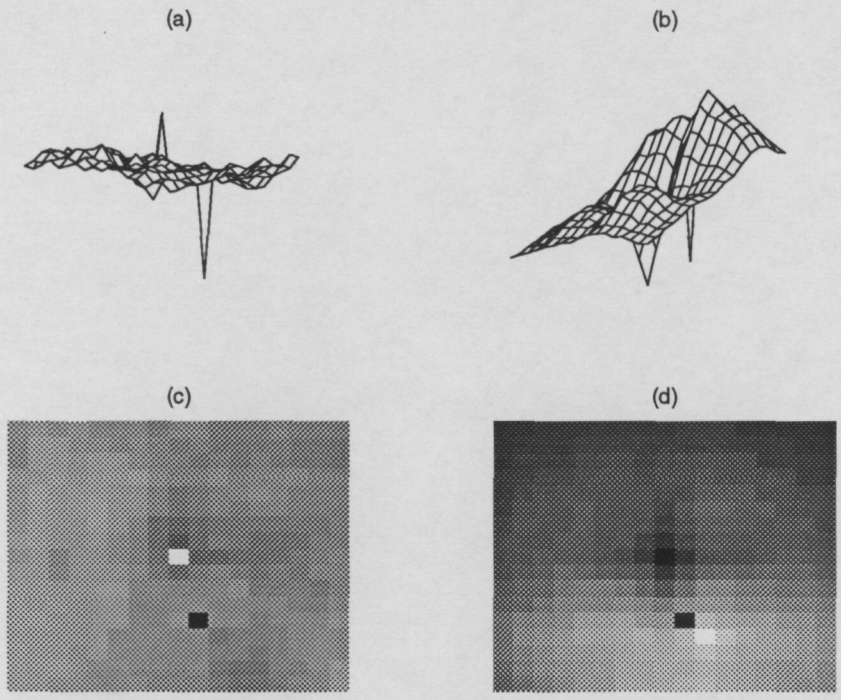

Fig 4.18 Estimated cost functions for a 2D white object of size=16x16 where $\boldsymbol{d}_{k-1}^{O}$= *(0,0)*, $\boldsymbol{d}_{k}^{O}$= *(4,1), SNR = 0 dB* from 20 runs a) 3-D view of $J_{42k}(\boldsymbol{d})$; b) $J_{2k}(\boldsymbol{d})$; c) image view of $J_{42k}(\boldsymbol{d})$; d) $J_{2k}(\boldsymbol{d})$.

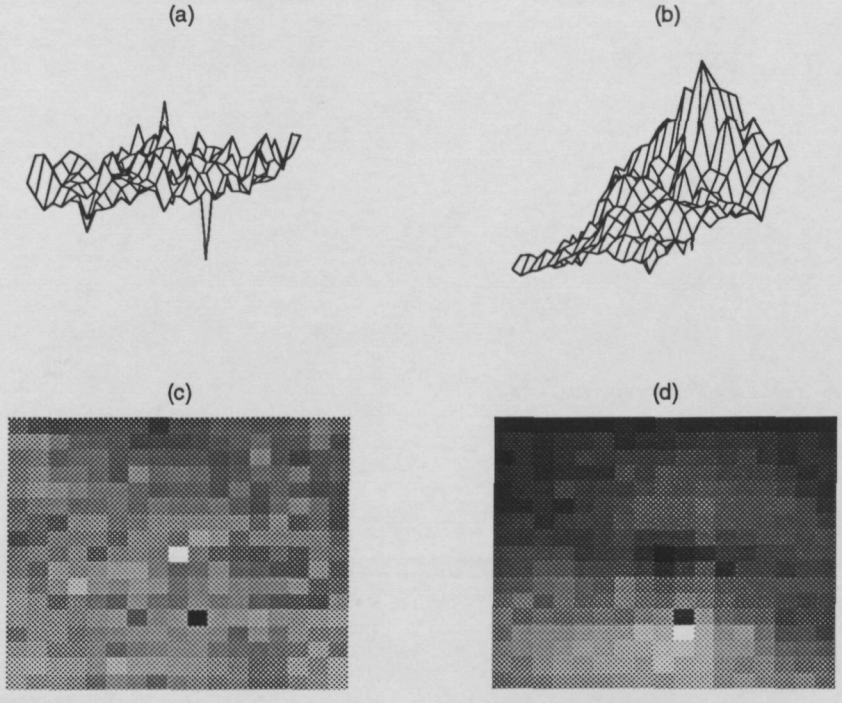

Fig 4.19 Estimated cost functions for a 2D white object of size=16x16 where $\boldsymbol{d}_{k-1}^{O}$= *(0,0)*, $\boldsymbol{d}_{k}^{O}$= *(4,1), SNR = 0 dB* for a single realization a) 3-D view of $J_{42k}(\boldsymbol{d})$; b) $J_{2k}(\boldsymbol{d})$; c) image view of $J_{42k}(\boldsymbol{d})$; d) $J_{2k}(\boldsymbol{d})$.

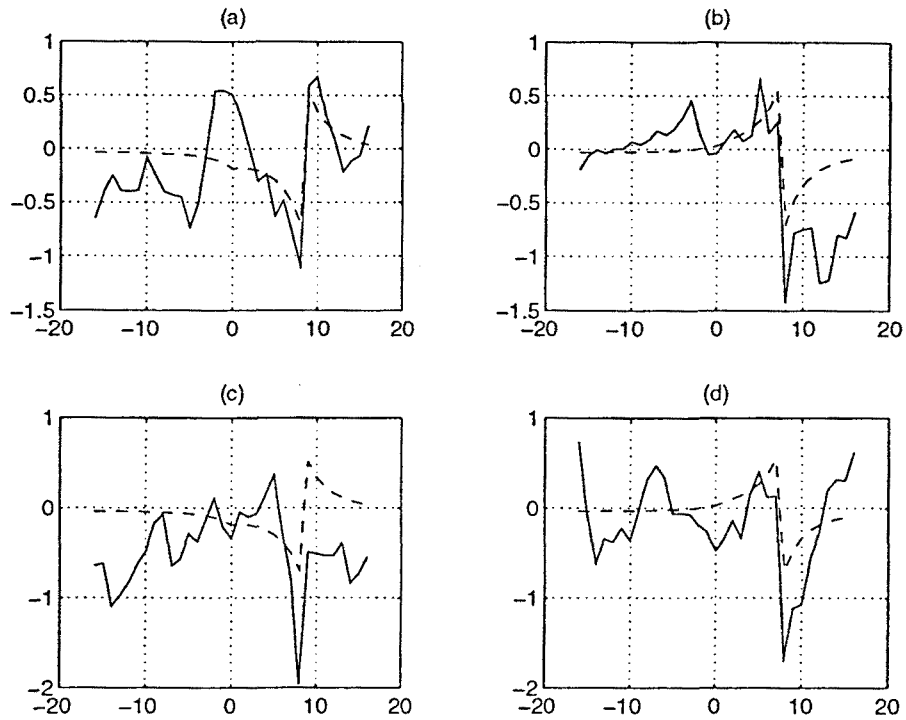

Fig 4.20 $J_{42k}(d)$ when $d_{k-2}^{o} = 0$ a) $\mu = 1$ $d_k^{o} = 8$, $d_{k-1}^{o} = 7$, b)$\mu = 1$ $d_k^{o} = 8$, $d_{k-1}^{o} = 9$, c) $\mu = 0.89$ $d_k^{o} = 8$, $d_{k-1}^{o} = 7$ d) $\mu = 0.89$ $d_k^{o} = 8$, $d_{k-1}^{o} = 9$.

size	32x32	16x16	32x32	16x16	32x32	16x16
SNR	0 dB	0 dB	-2 dB	-2 dB	-5 dB	-5 dB
$J_{42k}(d)$	0%	10%	10%	30%	80%	90%
$J_{2k}(d)$	0%	20%	40%	40%	100%	100%

Table 4.1 Percentage of error for example 4.6

4.4.4 Simple Version of the Modified Kurtosis of the DFD

The modified kurtosis cost function displays an outstanding behavior specially when d_k^o is different from d_{k-1}^o or, in case these displacements are similar, when we center the update or use $\mu<1$. The main improvement is that $J_{42k}(d)$ exhibits a low variance as compared to the kurtosis cost function, allowing smaller size signals or regions. On the other side, this new cost function is able to obtain the correct displacement when the SNR is low and second-order statistics of the DFD lead to ambiguous results. We are interested in defining a cost function with the characteristics of $J_{42k}(d)$ even though only two frames are available. This could be achieved if we replace $E\{DFD_{k-1}^2(d)\}$ for a convenient function. We choose the square differences of one of the frames with the same frame shifted d. The resulting cost function shows a behavior analogous to $J_{42k}(d)$ when $d_{k-1}^o=0$, that is, a maximum at displacement zero and a minimum at the current displacement. It was defined in Eq. (4.38) and we repeat it here for convenience.

$$\hat{J}_{43k}(d) = \frac{1}{\hat{J}_{2k}^2(d)} \frac{1}{N} \sum_{m\varepsilon\Omega_m} DFD_k^4(d) - 3\frac{1}{N}\sum_{m\varepsilon\Omega_m}[g_{k-1}(m) - g_{k-1}(m-d)]^2 \frac{1}{N} \sum_{m\varepsilon\Omega_m} DFD_k^2(d)$$

As we did for the other cost functions we have developed $J_{43k}(d)$ as a function of signal and noise moments, obtaining (Appendix D):

$$J_{43k}(d)= \frac{1}{J_{2k}^2(d)}$$

$$\{2m_{f4}+6E\{f_k^2(m)f_k^2(m+d_k^o-d)\}-4E\{f_k^3(m)f_k(m+d_k^o-d)\}-4E\{f_k(m)f_k^3(m+d_k^o-d)\}$$

$$-3\,[2\sigma_n^2-2r_{n1}(d)]^2+6[2\sigma_f^2-2r_f(d-d_k^o)]\,[2\sigma_n^2-2r_{n1}(d)]$$

$$-3[2\sigma_f^2-2r_f(d)+2\sigma_n^2-2r_{n0}(d)]\,[2\sigma_f^2-2r_f(d-d_k^o)+2\sigma_n^2-2r_{n1}(d)] \qquad (4.45)$$

The following examples will illustrate the response of this cost function.

Example 4.6 : In this example $J_{42k}(d)$ *and* $J_{43k}(d)$ are estimated in an analogous scenario than the previous examples and are found to look very similar. The performance indexes are compared for a 1-D colored rectangular object of length 256, which is moving along three frames where $d_{k-1}^o = 0$ and $d_k^o = 3$. For this case we choose a signal with positive kurtosis generated from a first-order AR system which coefficient is $b_m = 0.8$ and which input is a Laplacian distributed signal. Noise is simulated using an AR model with $a_m=a_k = 0.6$ and

SNR = -2 *dB*. We generate the sequence 20 times and compute the percentage of error for each cost function. Thus, we estimated 95 % of error using $J_{2k}(d)$, 100% of error for $J_{41k}(d)$, 45 % for $J_{42k}(d)$ and 50% using $J_{43k}(d)$. Figure 4.21 depicts each cost function for a single realization.

As we just mentioned, we observe that $J_{42k}(d)$ resembles $J_{43k}(d)$. Nevertheless, we have to keep in mind that whereas the latter is just an approximation that works correctly up to a certain *SNR*, the former does not change its behavior for low *SNR*, like the kurtosis. Figure 4.22 shows the theoretical mean curves for the two cost functions when the *SNR* is *0 dB*. On the other hand when the *SNR* tends to $-\infty$, $J_{42k}(d)$ does not change its shape while $J_{43k}(d)$ does not show a minimum anymore, see fig. 4.23.

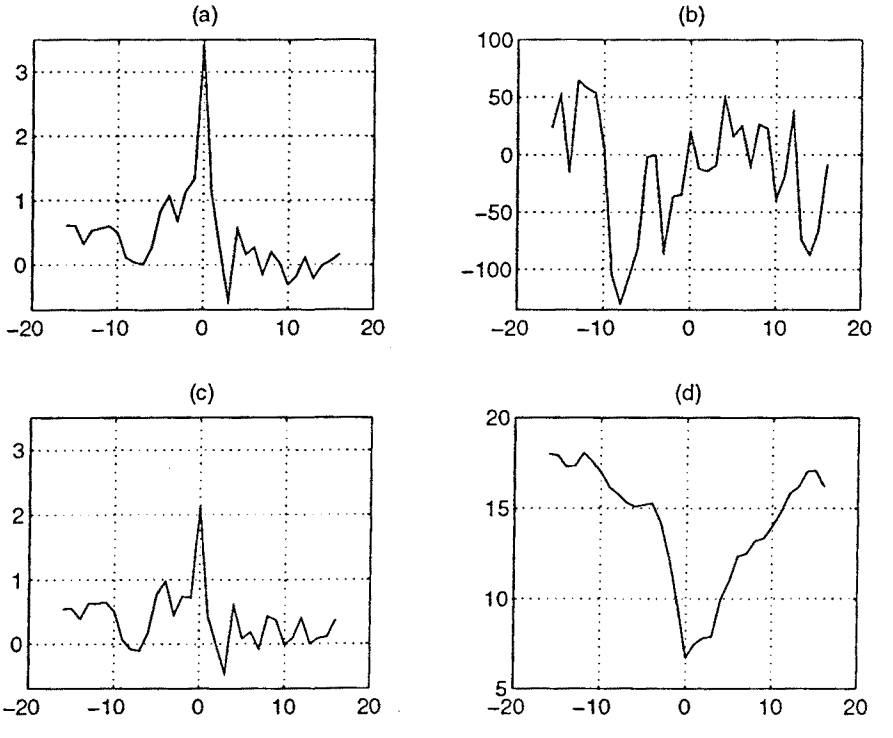

Fig 4.21 Cost functions for a single realization when $d_{k-1}^{o} = 0$, $d_k^{o} = 8$ *and SNR* = -2 *dB* for a colored signal of length 256 and positive kurtosis: a) $J_{43k}(d)$; b)$J_{41k}(d)$; c) $J_{42k}(d)$; d)$J_{2k}(d)$

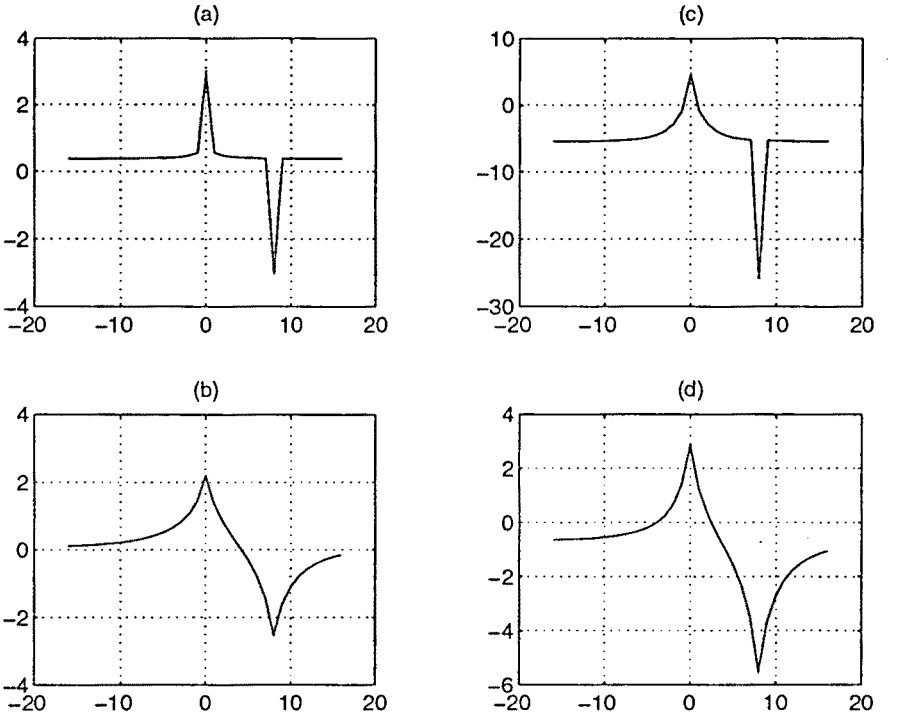

Fig 4.22 Theoretical behavior of the cost functions when $d_{k-1}^{o} = 0$, $d_k^{o} = 8$ and $SNR = 0\ dB$ for a white signal a) $J_{42k}(d)$; c) $J_{43k}(d)$; and a correlated signal b) $J_{42k}(d)$; d) $J_{43k}(d)$

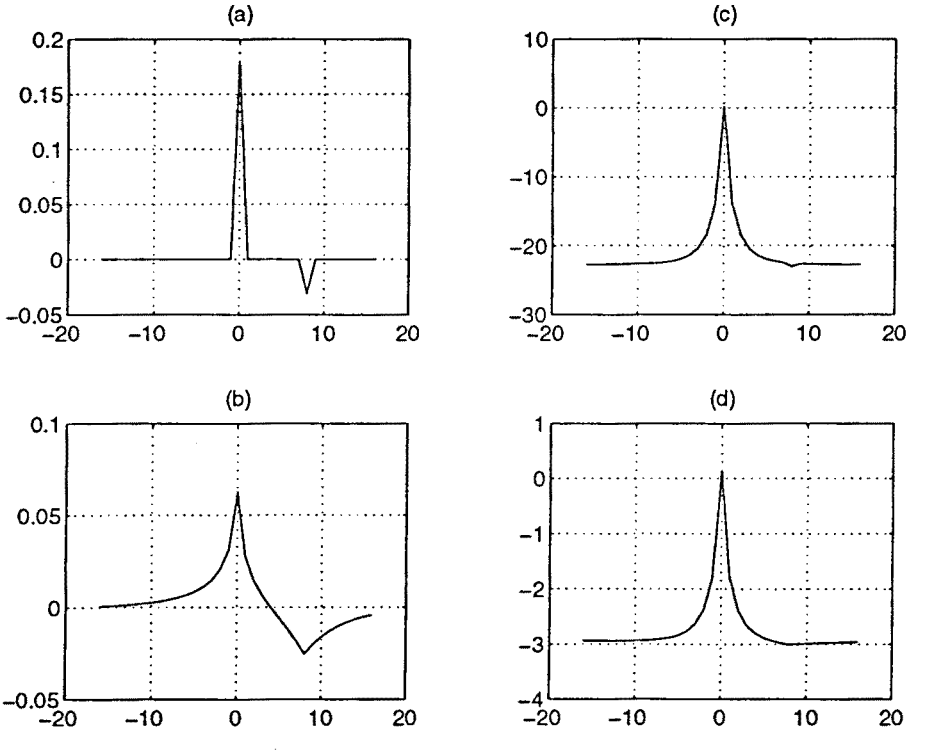

Fig 4.23 Theoretical behavior of the cost functions when $d_{k-1}^{o} = 0$, $d_k^{o} = 8$ and $SNR = -30\ dB$ for a white signal a) $J_{42k}(d)$; c)$J_{43k}(d)$; and a correlated signal b) $J_{42k}(d)$; d)$J_{43k}(d)$

Example 4.7: The cost function $J_{43k}(d)$ has applicability in a different context involving time delay estimation. Hinich et al. [1989] have shown via bispectral analysis that whereas the ambient ocean noise is indeed Gaussian, the ship radiated noise is non-Gaussian. Thus, the use of higher-order statistics for the time delay estimation in passive sonar is well-motivated. On the other side, Tugnait, [1991], proposed an optimization approach where the time delay between two signals is estimated by minimizing a mean fourth-order (MFC) criterion, which is nothing else than $J_{41k}(d)$. To demonstrate its performance he used the following example. Time delay between two 1-D signals has to be estimated. The signal is given by the product $f_{k-1}(m) = W_{k-1}(m)\,\beta_{k-1}(m)$ where $W_{k-1}(m)$ is Laplace i.i.d and $\beta_{k-1}(m)$ is a Bernoulli process. This type of signal is a test signal widely used in the acoustics/ geophysics literature (a lot of controversy exist whether or not it approximates a real signal). The noise sources are spatially correlated, $n_{k-1}(m)$ is generated first, whereas $n_k(m)$ is computed from

$$n_k(m) = \sum_{i=0}^{10} b(i)\, n_{k-1}(m+i) \tag{4.41}$$

where $b(i)$ takes the values {0.2, 0.4, 0.6, 0.8, 1, 1, 1, 0.7, 0.5, 0.3, 0.1}. It was seen that $J_{41k}(d)$ yields the true time delay, that was set to $d_k^o=16$, whereas $J_{2k}(d)$ does not. The signal length was 2000 and the $SNR = -5\ dB$. In addition, the newly developed cost function $J_{43k}(d)$ can also be used to obtain the true time delay. Figs. (4.24a), (4.24b) and (4.24c) show the mean plus/minus standard deviation of the three cost functions for 10 realizations. Figures (4.25a), (4.25b) and (4.25c) show the cost functions for a signal of length 64 for 10 realizations. We obtained 90% of error for $J_{41k}(d)$ versus 20% of error for $J_{42k}(d)$. We can then conclude that the new cost function outperformed the variance and the unnormalized kurtosis cost functions.

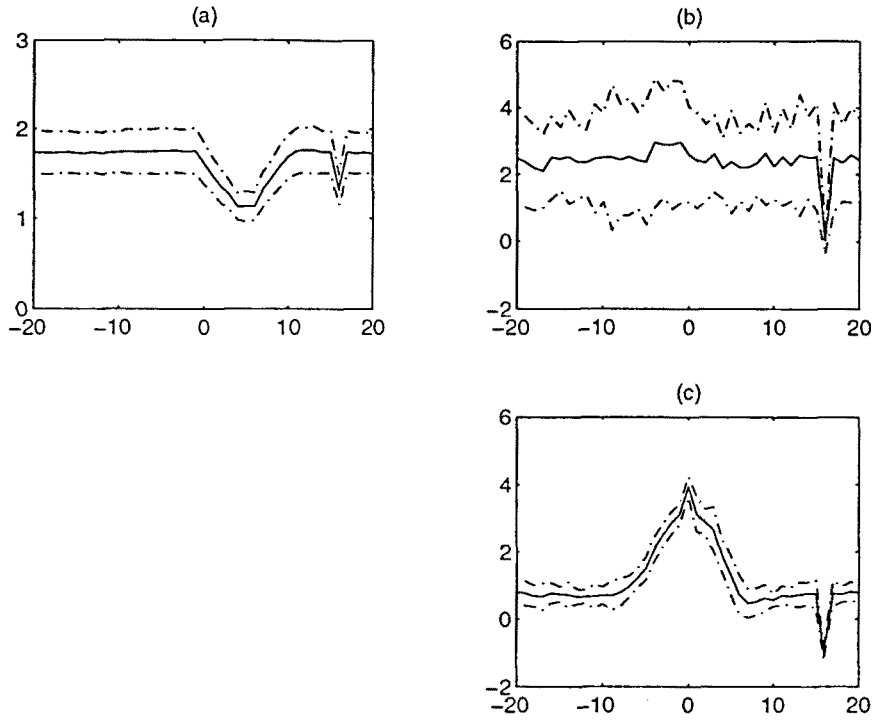

Fig. 4.24 a) mean behavior of $J_{2k}(d)$ for a 1-D signal of length 2000 and *SNR* = *-5 dB* b) $J_{41k}(d)$ c) $J_{42k}(d)$

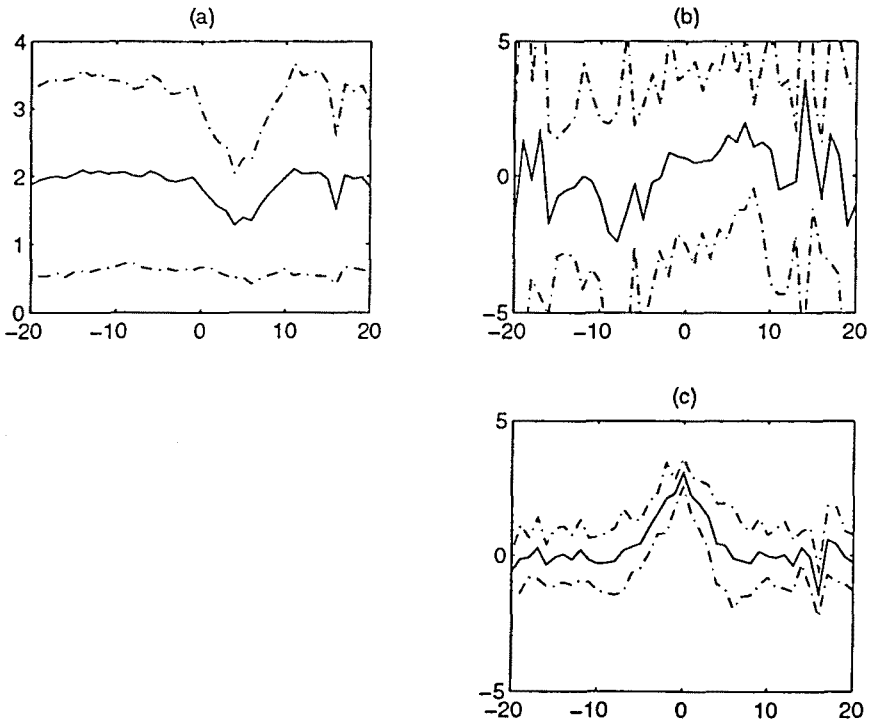

Fig. 4.25 a) mean behavior of$J_{2k}(d)$ for a 1-D signal of length 64 and *SNR* = *-5 dB* b) $J_{41k}(d)$ c) $J_{42k}(d)$

Example 4.8: This example demonstrates the improvement of the new fourth-order based cost function $J_{43k}(\boldsymbol{d})$ from the second-order one, $J_{2k}(\boldsymbol{d})$, when block-matching is applied to obtain the displacement between consecutive real frames. Figure 4.26a shows one of the original images taken from the "flowers" sequence. Figure 4.26b is the same image when colored Gaussian noise generated from an AR model with $a_k = a_m = a_n = 0.6$ has been added to the sequence and the SNR is 2 dB. In first place we have manually displaced by (4,0) all pixels in the image. Figure 4.27a depicts the ideal vector displacement map given blocks of 16x16 pixels. The result for noisy frames when using the correlation-based measure is shown in fig. 4.27b. Most blocks are represented by a dot point that indicates that displacement zero has been detected. Figure 4.27c shows the results after applying $J_{43k}(\boldsymbol{d})$. As a whole, we observe that the detection decision has been improved. Notice that most wrong decisions are located in the upper part of the image where the homogeneous sky is, whereas most correct decisions are located on the flower zone which is a textured region. The percentage of correct decisions for $J_{43k}(\boldsymbol{d})$ is 17% and 7% for $J_{2k}(\boldsymbol{d})$. Another important measure of *closeness* is derived when the difference of the computed from the correct displacement is less or equal than one pixel. Thus, a 37% of closeness is obtain for $J_{43k}(\boldsymbol{d})$ versus a 7 % for $J_{2k}(\boldsymbol{d})$.

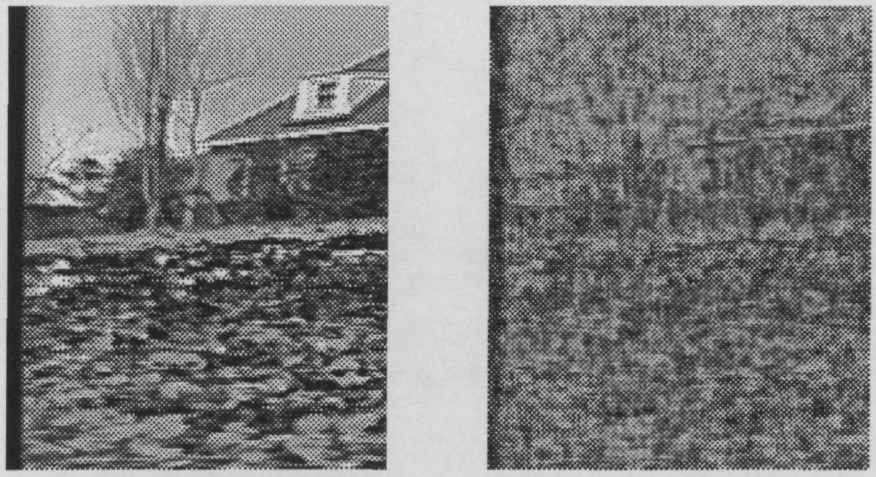

(a) (b)

Fig 4.26 a) one of the original frames from the flowers sequence b) one of the noisy frames where colored noise follows an AR model with $a_k = a_m = a_n = 0.6$ and the SNR is 2 dB.

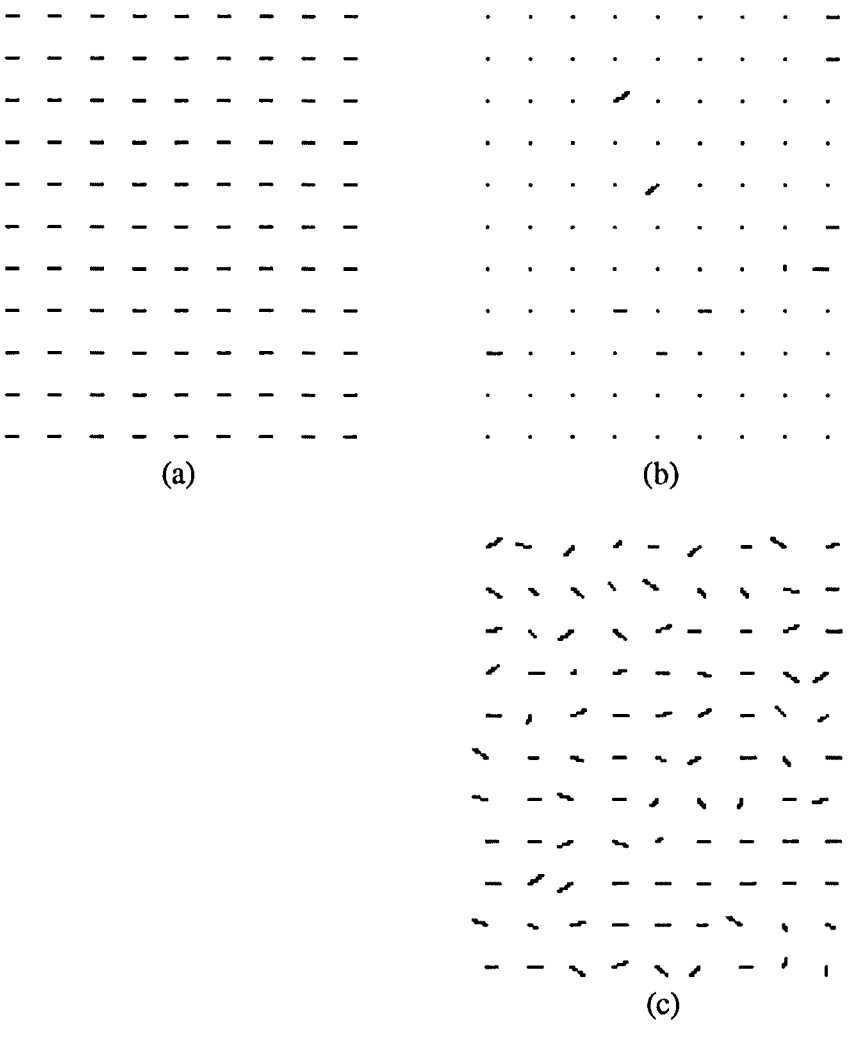

Fig 4.27 a) Noise-free displacement map given blocks of 16x16 pixels after applying $J_{2k}(\boldsymbol{d})$, where all pixels in the second frame have been displaced by (4,0) b) map for noisy frames using $J_{2k}(\boldsymbol{d})$. c) using $J_{43k}(\boldsymbol{d})$.

In second place, real displacement from two consecutive frames of the "flowers" sequence (frames 112 and 113), is computed. The results obtained from the second-order cost function when no noise is added is illustrated in fig 4.28a. Some blocks from the left hand side of the image as well as some blocks containing pixels from the sky seem to be wrongly detected. Figure 4.28b and 4.28c are the maps obtained when colored noise is added to the sequence for $J_{2k}(\boldsymbol{d})$ and $J_{43k}(\boldsymbol{d})$ respectively. As expected the fourth-order cost function outperforms the second-order one. In this case we obtain a 23% of correct decision for $J_{43k}(\boldsymbol{d})$ versus 12% for $J_{2k}(\boldsymbol{d})$. The closeness measure results in a 37% for $J_{43k}(\boldsymbol{d})$ versus 19% for $J_{2k}(\boldsymbol{d})$.

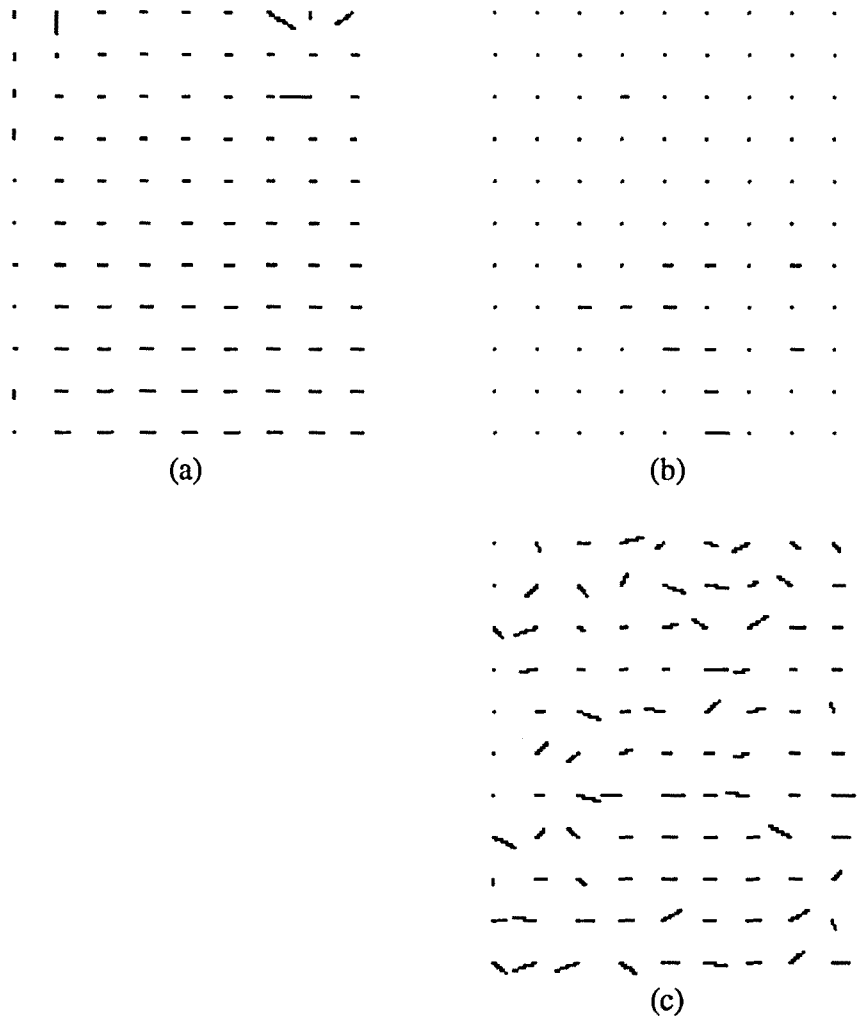

Fig 4.28 a) Noise-free real displacement map given blocks of 16x16 pixels obtained from $J_{2k}(\boldsymbol{d})$. b) displacement map for noisy frames when using $J_{2k}(\boldsymbol{d})$ c) using $J_{43k}(\boldsymbol{d})$.

Motion estimation is also computed when applying region-matching to previously segmented images. Segmentation is only performed over the first image of the sequence, see fig. 4.29a, using a multiresolution method that applies morphological filters in each resolution level [Salembier & Pardàs, 1994]. This method is chosen since morphological filters are visually satisfactory and are not based on Gaussianity concepts. The displacement map of the regions from two consecutive frames when utilizing $J_{2k}(\boldsymbol{d})$ is shown in fig. 4.29b for the noise-free case. In case the sequence is corrupted by colored Gaussian noise the results after applying $J_{2k}(\boldsymbol{d})$ and $J_{43k}(\boldsymbol{d})$ are illustrated in figs. 4.29c and 4.29d respectively. The AR model

parameters are $a_k=a_m=a_n= 0.6$ and the SNR is 2 dB. The detection map is slightly better for the fourth-order cost function. Nevertheless, the results are poorer to the ones obtained for the block-matching approach.

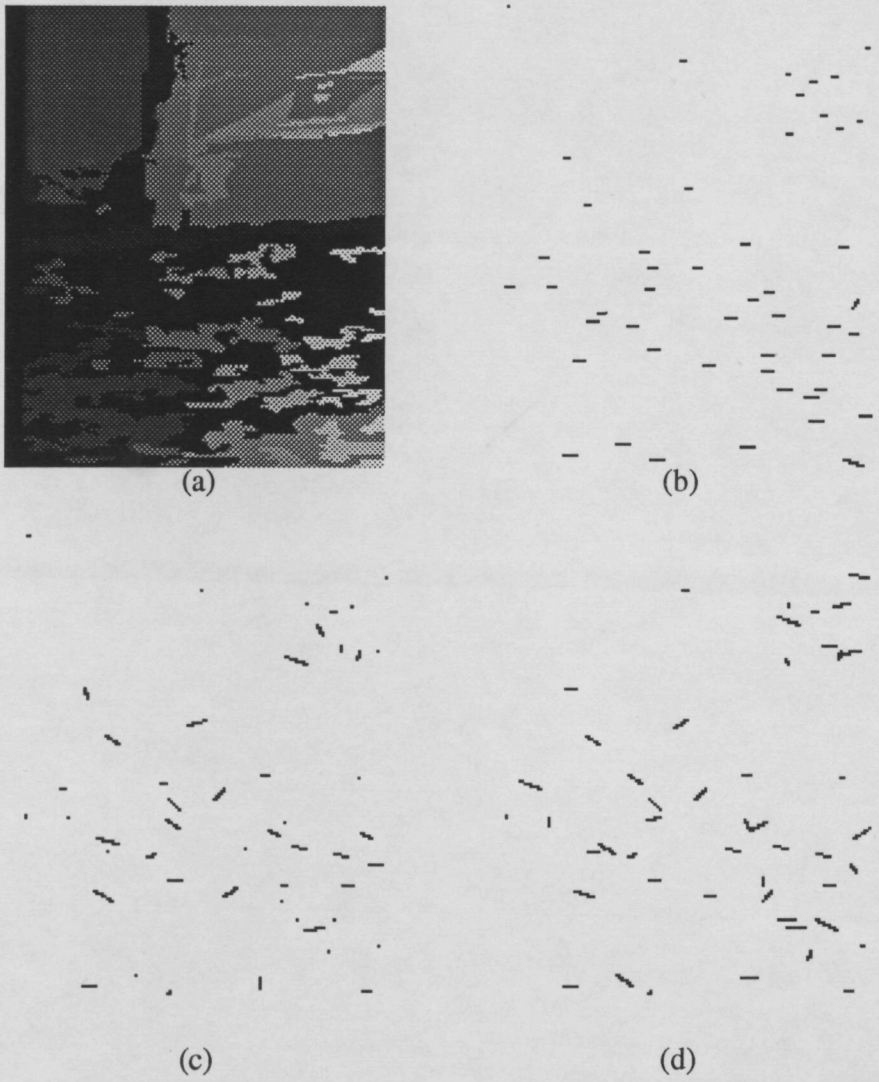

Fig 4.29 a) Segmentation of image 4.26a b)displacement map for the noise-free case using $J_{2k}(\boldsymbol{d})$. b) displacement map for noisy frames when using $J_{2k}(\boldsymbol{d})$. c) and using $J_{43k}(\boldsymbol{d})$.

4.5 Recursive estimation of the displacement

In the previous sections the estimated displacement was taken from an exhaustive search of the displacement that provided the absolute minimum or maximum of a given cost function. Recursive estimation algorithms aim to reduce the computational complexity, specially for sub-pixel displacements, since they use a priori information on the location of regions. Thus, given an i^{th} estimate of displacement, we obtain the $(i+1)^{th}$ estimate such that, the value of the cost function resulting from the $(i+1)^{th}$ estimate is lower (or higher) than the one used in the i^{th}. The gradient search procedure is represented algebraically as :

$$d^{\,i} = d^{\,i-1} - \varepsilon\, sgn[\gamma(d^{\,i-1})]\ \nabla_{d^{i-1}}\ J(d^{\,i-1}), \tag{4.42}$$

where $d^{\,i}$ is the estimated displacement at the i^{th} iteration, ε is a constant, $\nabla_{d^{i-1}}$ is the gradient with respect to the estimated displacement and finally, $\gamma(d^{\,i-1})$ gives the correct sign for every cost function and statistics of the signal of interest.

4.5.1 Recursive Estimation based on the variance of the *DFD*

Netravali & Robbins [1979] were the first to use a gradient type approach to obtain the displacement vector from the variance of the *DFD*. The recursive formulation becomes

$$d^{\,i} = d^{\,i-1} - \varepsilon\ \nabla_{d^{i-1}}\ E\{DFD_k{}^2(d^{\,i-1})\},$$

$$d^{\,i} = d^{\,i-1} - \varepsilon\, E\{2\ DFD_k(d^{\,i-1})\, \nabla_{d^{i-1}}\, DFD_k(d^{\,i-1})\}. \tag{4.43}$$

For this cost function the goal is to reach a minimum, and then $sgn[\gamma(d^{\,i-1})]$ is always 1. Substituting the *DFD* by the signal difference, the gradient of the *DFD* may be computed from the gradient of the image intensity since $\nabla_{d^{i-1}}\, DFD_k(d^{\,i-1}) = \nabla_m\, g_k(m+d_k^{\,o}-d^{\,i-1})$. Then it follows :

$$d^{\,i} = d^{\,i-1} - \varepsilon\, E\{2\ DFD_k(d^{\,i-1})\ \nabla_m\, g_k(m+d_k^{\,o}-d^{\,i-1})\}. \tag{4.44}$$

This expression must be estimated for the displacement of regions between frames. We utilize the estimation we defined in Eq. (4.5), which yields to:

$$d^{\,i} = d^{\,i-1} - 2\,\varepsilon \frac{1}{N} \sum_{m \varepsilon \Omega_m} DFD_k(d^{\,i-1})\ \nabla_m g_k(m+d_k^{\,o}-d^{\,i-1}). \tag{4.45}$$

The above recursive motion estimator was successfully applied to simulated and real image

sequences. It was also evaluated in the context of frame-to-frame coding [Netravali, 1979]. Its performance will be compared to the recursive version of the new-defined cost function.

4.5.2 Recursive estimation based on the kurtosis of the *DFD*, $J_{41k}(d)$

The recursive estimation based on the kurtosis of the *DFD* was developed by Anderson [1994]. It is given by:

$$d^{i} = d^{i-1} - \varepsilon\, sgn[\gamma(d^{i-1})]\ \nabla_{d\,i-1}[E\{DFD_k^4(d^{i-1})\}-3E^2\{DFD_k^2(d^{i-1})\}]$$

$$d^{i} = d^{i-1} - \varepsilon\, sgn[\gamma(d^{i-1})]$$

$$[E\{\,4\,DFD_k^3(d^{i-1})\,\nabla_m g_k(m+d_k^o-d^{i-1})\,\}$$

$$-\,6E\{DFD_k^2(d^{i-1})\}\ E\{\,2DFD_k(d^{i-1})\ \nabla_m g_k(m+d_k^o-d^{i-1})\}\,] \qquad (4.46)$$

In this case $sgn[\gamma(d^{i-1})] = sgn[\,K(f_k(m))]$, that is, it is positive for distributions with positive kurtosis and negative for regions of negative kurtosis. Likewise we use the estimation in Eq. (4.17) and obtain,

$$d^{i} = d^{i-1} - \varepsilon\, sgn[K(f_k(m))]$$

$$\Big[\frac{1}{N}\sum_{m\varepsilon\Omega_m} 4\,DFD_k^3(d^{i-1})\,\nabla_m g_k(m+d_k^o-d^{i-1})$$

$$-12\,\frac{1}{N}\sum_{m\varepsilon\Omega_m} DFD_k^2(d^{i-1})\ \frac{1}{N}\sum_{m\varepsilon\Omega_m} DFD_k(d^{i-1})\ \nabla_m g_k(m+d_k^o-d^{i-1})\,\Big] \qquad (4.47)$$

The recursive equation for the cost function based on the kurtosis of the DFD was compared to the second-order recursive estimator [Anderson, 1994]. It is shown there that there is an improvement when the image frames are corrupted by colored noise. However the comparison was carried out for local neighborhoods, where only three to six pixels are involved, and therefore statistical models are not valid.

4.5.3 Recursive estimation based on the modified kurtosis of the *DFD*

As we saw for the exhaustive estimation of motion, the kurtosis is characterized by a large variance and the *ideal shape* of the cost function is not achieved in single realizations for moderate size signals. The second-order cost function may lead to the true solution if we are close enough from the local minimum that appears at the correct displacement. This local

minimum is only observable when the SNR is not very low. See for example figure 4.16, where we can observe that $J_{2k}(d)$ displays a maximum between displacement zero and d_k^o. In this case if the starting point in the recursive algorithm is on the right side of this maximum or on the right side of d_k^o the gradient recursive algorithm will reach the correct displacement. The same figure shows $J_{42k}(d)$. For this cost function a gradient type of approach will lead to the correct displacement from a starting point lying further from the correct solution. In other situations, like the one shown in figure 4.21 of Example 4.6 the right solution using $J_{2k}(d)$ may never be reached whereas for $J_{42k}(d)$ a gradient-based algorithm may lead to the right solution

The recursive estimation formula is an expression rather complex since the cost function is normalized to $J_{42k}(d)$. It is given by:

$$d^{i} = d^{i-1} - \varepsilon \cdot \nabla_{d^{i-1}} \frac{[E\{DFD_k^4(d^{i-1})\} - 3E\{DFD_k^2(d^{i-1})\}E\{DFD_{k-1}^2(d^{i-1})\}]}{E^2\{DFD_k^2(d^{i-1})\}} \qquad (4.48)$$

In this case $sgn[\gamma(d^{i-1})] = 1$ since we are looking for a minimum independently of the sign of the kurtosis. This might represent an advantage in cases where the sign of the kurtosis of the region might be unknown. The gradient of the *DFD* at time $k-1$ may be as well expressed as a function of the image intensity at time k considering the displacement of the region.

$$\nabla d^{i-1}\, DFD_{k-1}(d^{i-1}) = \nabla m\, g_k(m+d_{k-1}^o - d^{i-1}) \qquad (4.49)$$

and the recursive formulation becomes,

$$d^{i} = d^{i-1} - \varepsilon \frac{1}{E^4\{DFD_k^2(d^{i-1})\}}$$

$$[\; E\{4DFD_k^3(d^{i-1})\nabla_m g_k(m+d_k^o - d^{i-1})\}E^2\{DFD_k^2(d^{i-1})\}$$

$$-3E\{DFD_{k-1}^2(d^{i-1})\}E\{2DFD_k(d^{i-1})\nabla_m g_k(m+d_k^o - d^{i-1})\}E^2\{DFD_k^2(d^{i-1})\}$$

$$-3E\{DFD_k^2(d^{i-1})\}E\{2DFD_{k-1}(d^{i-1})\nabla_m g_k(m+d_{k-1}^o - d^{i-1})\}E^2\{DFD_k^2(d^{i-1})\}$$

$$-2E\{DFD_k^2(d^{i-1})\}E\{2DFD_k(d^{i-1})\nabla_m g_k(m+d_k^o - d^{i-1})\}$$

$$\cdot[E\{DFD_k^4(d^{i-1})\} - 3E\{DFD_k^2(d^{i-1})\}E\{DFD_{k-1}^2(d^{i-1})\}] \;] \qquad (4.50)$$

The following step is to substitute the expectation operators by the estimation in eq. (4.35) obtaining:

$$d^{i} = d^{i-1} - \varepsilon \left[\frac{1}{N} \sum_{m\varepsilon\Omega_m} DFD_k^2(d^{i-1}) \right]^{-4}$$

$$\left[4 \frac{1}{N} \sum_{m\varepsilon\Omega_m} DFD_k^3(d^{i-1}) \nabla_m g_k(m+d_k^o-d^{i-1}) \left[\frac{1}{N} \sum_{m\varepsilon\Omega_m} DFD_k^2(d^{i-1}) \right]^2 \right.$$

$$-6 \frac{1}{N} \sum_{m\varepsilon\Omega_m} DFD_{k-1}^2(d^{i-1}) \frac{1}{N} \sum_{m\varepsilon\Omega_m} DFD_k(d^{i-1}) \nabla_m g(m+d_k^o-d^{i-1}) \left[\frac{1}{N} \sum_{m\varepsilon\Omega_m} DFD_k^2(d^{i-1}) \right]^2$$

$$-6 \frac{1}{N} \sum_{m\varepsilon\Omega_m} DFD_k^2(d^{i-1}) \frac{1}{N} \sum_{m\varepsilon\Omega_m} DFD_{k-1}(d^{i-1}) \nabla_m g_k(m+d_{k-1}^o-d^{i-1}) \left[\frac{1}{N} \sum_{m\varepsilon\Omega_m} DFD_k^2(d^{i-1}) \right]^2$$

$$-4 \frac{1}{N} \sum_{m\varepsilon\Omega_m} DFD_k^2(d^{i-1}) \frac{1}{N} \sum_{m\varepsilon\Omega_m} DFD_k(d^{i-1}) \nabla_m g_k(m+d_{k-1}^o-d^{i-1})$$

$$\left. \left[\frac{1}{N} \sum_{m\varepsilon\Omega_m} DFD_k^4(d^{i-1}) - 3 \frac{1}{N} \sum_{m\varepsilon\Omega_m} DFD_k^2(d^{i-1}) \frac{1}{N} \sum_{m\varepsilon\Omega_m} DFD_{k-1}(d^{i-1}) \right] \right] \qquad (4.51)$$

which is rewritten as :

$$d^{i}=d^{i-1}-\varepsilon \left[\frac{1}{N} \sum_{m\varepsilon\Omega m} DFD_k^2(d^{i-1}) \right]^{-2} \left[4 \frac{1}{N} \sum_{m\varepsilon\Omega m} DFD_k^3(d^{i-1}) \nabla_m g_k(m+d_k^o-d^{i-1}) \right.$$

$$+6 \frac{1}{N} \sum_{m\varepsilon\Omega m} DFD_{k-1}^2(d^{i-1}) \frac{1}{N} \sum_{m\varepsilon\Omega m} DFD_k(d^{i-1}) \nabla_m g_k(m+d_k^o-d^{i-1})$$

$$-6 \frac{1}{N} \sum_{m\varepsilon\Omega m} DFD_k^2(d^{i-1}) \frac{1}{N} \sum_{m\varepsilon\Omega m} DFD_{k-1}(d^{i-1}) \nabla_m g_k(m+d_{k-1}^o-d^{i-1})$$

$$\left. - \quad 4 \frac{1}{N} \sum_{m\varepsilon\Omega m} DFD_k(d^{i-1}) \nabla_m g_k(m+d_{k-1}^o-d^{i-1}) \frac{1}{N} \sum_{m\varepsilon\Omega m} DFD_k^4(d^{i-1}) \left[\frac{1}{N} \sum_{m\varepsilon\Omega m} DFD_k^2(d^{i-1}) \right]^{-1} \right]$$

(4.52)

This expression looks rather complex since it involves five terms instead of the two used for the kurtosis. This is mainly due to the normalization factor. Nevertheless, the terms involving previous frames, like the variance of the DFD at time k-1, do not have to be computed again.

Despite an increase in the computational load, the results are satisfactory as it was for the exhaustive search. The following example illustrates the improvement.

Example 4.8. We compare the recursive schemes of $J_{42k}(d)$ and $J_{2k}(d)$, for a situation similar to example 4.5. The object in this case, is a 2-D uniformly distributed rectangular object of size 16x16 which pixels are correlated following a first order AR model. We generated 10 realizations of a sequence of 3 images for three different SNR. The object is moving (3,1) pixels per frame. For the first pair of images the objective is to estimate the displacement when an initial guess is provided, using Eq. (4.38) in the recursive scheme. The initial position was (1,0) and ε was set to 0.2. The percentages of error after 20 iterations are given in Table 4.2. The second-order cost function often leads to a local minimum at (0,0). On the other hand, for the second pair of images the correct previous displacement was given and the objective was to check if the cost functions were able to track the minimum, the results are given in Table 4.3. For very low SNR, $J_{42k}(d)$ is characterized by a 50% of error whereas $J_{2k}(d)$ always failed.

SNR	0 dB	-2 dB	-5 dB
$J_{42k}(d)$	10%	30%	50%
$J_{2k}(d)$	90%	90%	100%

Table 4.2 Percentage of error to reach minimum given an initial guess, example 4.8.

SNR	0 dB	-2 dB	-5 dB
$J_{42k}(d)$	0%	30%	50%
$J_{2k}(d)$	10%	30%	100%

Table 4.3 Percentage of error in tracking given the correct previous displacement, example 4.8

4.6 Conclusions and final remarks

There are some situations where motion between frames has to be estimated in the presence of noise. In such cases most existing methods do not work properly and more robust techniques are necessary. On the other hand, noise can be realistically described as a colored Gaussian process. In such circumstances, HOS may offer some advantages since cumulants of Gaussian processes are asymptotically zero. In this chapter, a two-step motion estimation scheme has been proposed. In the first step, the images are divided in blocks or regions. In the second one, a cost function estimates the displacement of these blocks or regions. Cost functions of the *displaced frame difference* based on second and fourth-order statistics were examined and compared. For this purpose, analytical expressions were derived from AR models of the image regions and noise.

The theoretical study showed the following results:

- The second-order statistics function of the DFD is capable of detecting the correct displacement from an absolute minimum up to certain SNR which varies depending on the correlation of the noise and signal.

- The kurtosis of the DFD is capable of detecting the correct displacement from an absolute minimum or maximum, depending on the sign of the kurtosis of the region, for any SNR.

- A new fourth-order function of the DFD was also defined. This cost function is based on an adaptive scheme for the estimation of fourth-order cumulants and uses previous frames to estimate motion. It shows a minimum at the correct displacement and a maximum at displacement zero independently of the sign of the kurtosis. The theoretical study shows that the shape of the cost function is affected by the noise covariance function. Its influence is however positive since the shape of the cost function is accentuated and not distorted by the noise.

Simulations employing moderate size regions and low SNR were given. The following conclusion can be drawn out:

- The mean of the second-order cost function of the DFD obeyed the theoretical values with low variance.

- The mean behavior of the kurtosis followed the predicted function, however its variance was so high that detection of the correct displacement was difficult in most of the cases. This measure should only be utilized for long data records which imply moderate variance.

- The modified kurtosis of DFD followed the theoretical results and the correct displacement could be easily detected in some cases where the two previous measures could not. The objective to obtain a HOS measure with lower variance estimates than the kurtosis was satisfied. The main problem of this cost function appeared for negative kurtosis regions when two consecutive displacements were the same. The behavior in this case was similar to the normalized kurtosis but could be easily improved by changing a parameter or shifting the previous update term.

This new-defined cost function shows its usefulness for moderate size regions in a range of SNR where the second-order cost function is biased and the kurtosis shows a high variance. For higher SNR it is reasonable to use the variance of the DFD since it is able to obtain the correct displacement at a lower cost. For very low SNR the variance of the new defined cost function increases and therefore, as the kurtosis, any improvement is manifested only for larger regions.

A simplified version when only two frames are available as well as a recursive version were also given. In particular, the fourth-order based cost function for only two frames was employed in an application unrelated to image processing that involved time delay estimation. The results showed an improvement with respect to existing techniques since the new method was capable of dealing with shorter signals. The recursive estimator behavior was also illustrated and outperformed the second-order statistics-based approach.

The results of this Chapter suggest that low-variance cost functions based on higher-order statistics may be defined and can outperform not only the second-order cost function but other existing HOS-based cost functions.

CHAPTER 5

CONCLUSIONS

In this thesis new applications of Higher-Order Statistics to two different image processing fields were developed. The major challenge of the two studied topics was to solve each particular problem when images had suffered a degradation phenomena of known statistics. In case this degradation consisted of additive colored Gaussian noise of unknown covariances and/or linear phase blurring filters some properties of HOS were particularly useful. That is, in contrast to second-order statistics, higher-order statistics are asymptotically unaffected by additive Gaussian noise. Another advantage is that phase information is preserved except for a constant factor. These properties were introduced in the first chapter of the thesis and exploited in the following chapters for each application.

In the first part of this work, the restoration of degraded images from the HOS of their projections was investigated.

Using projections of images has many advantages. First of all, the properties of the blurring function are preserved. Thus, if the 2-D PSF has zero or linear phase FT, its projections also have zero or linear phase FT. The convolution theorem is also valid for the projections. Second, the computational load applying HOS-based methods is reduced. Actually, this is the main motivation to use HOS over the projections.

Different algorithms were derived to reconstruct the 1-D signals from either the phase of the Fourier Transform or the phase of the Bispectrum. For this purpose, three Corollaries were established as the theoretical bases of the restoration strategy.

The algorithms were applied to images distorted with deterministic PSF and Gaussian noise and to simulated and real astronomical images degraded by turbulent atmosphere. The quality of the reconstructed images was considerably improved with respect to the original pictures. Some examples were also provided which showed better achievement with respect to other restoration schemes. The capability of the WS algorithm to reconstruct the projections from its third-order moments was demonstrated. The results proved to be quite good for moderate SNR. For low SNR the restoration of the projections was also good, although small errors in some of the projections are easily propagated to the image.

In the second part of the thesis the problem of Motion Estimation was examined when image frames are corrupted by colored Gaussian noise. A two-step motion estimation scheme was proposed. In the first step, the images are divided in blocks or regions. In the second one, a cost function estimates the displacement of these blocks or regions. Cost functions of the *DFD* based on second and fourth-order statistics for *AR* models of both the image regions and the noise were studied. The mean of the second-order cost function of the DFD obeyed the theoretical values with low variance. The mean behavior of the kurtosis followed the predicted function, however its variance was so high that detection of the correct displacement was difficult in most of the cases. These results were compared to a new HOS-based cost function. The modified kurtosis of DFD followed the theoretical results and the correct displacement could be easily detected in some cases where the two previous measures could not. The objective to obtain a HOS measure with lower variance estimates than the kurtosis was satisfied. The main problem of this cost function appeared for negative kurtosis regions when two consecutive displacements were the same. The behavior in this case was similar to

the normalized kurtosis but could be easily improved by changing a parameter or shifting the previous update term. This new-defined cost function showed the best behavior for moderate size regions in a range of *SNR* where the second-order cost functions are biased and the previously existing kurtosis criterion shows a high variance.

6.1 Topics for Future Research

Signal Processing as well as Image Processing research grows year by year considering techniques that were traditionally treated with second-order statistics. In most cases this improvement is well justified, however its practical application in some areas of image processing is arguable. The amount of data present in a single image is too small to extract information from higher-order statistics. Therefore, only research work that considers image series or sequences may really benefit from the properties of HOS. The price such techniques pay is a very high computational load. This is actually the main drawback of the restoration scheme we presented in this thesis, even though the restoration was performed over the projections of the image.

In my opinion, future work on the area of image restoration employing HOS, should be directed towards the following direction:

- As we have mentioned, small errors in the reconstruction of projections are easily propagated to the final image. This fact is accentuated when images are affected by low SNR even though the projections seem to be properly reconstructed. The only way to solve this problem is to avoid using projections for strongly degraded images. However, the analytical complexity grows considerably when the Bispectrum of an image (not the projections), which is a 4-D signal, is estimated. Therefore, future work should be directed towards low cost procedures to extract the signal information from the Bispectra of images as well as low cost restoration techniques that could make use of this information.

- A special case in this area is the restoration of astronomical images. Although this was one of the first applications in this area, many research groups are still currently working in this field. For example, in last European Signal Processing Conference (EUSIPCO '94) many works on astronomical images were presented [Negrete, 1994] [Rosille, 1994] . An interesting perspective was presented in [Negrete, 1994] that consisted on using adaptive optics techniques preprocessing together with bispectral processing to obtain highly accurate astronomical objects. This could be one future line of research. In my opinion also, other methods which are mostly based on the Phase of the Bispectrum should also be investigated.

On the other hand, in the area of motion estimation, future research in the line of this work can be extended in many interesting and important directions:

- The employment of parametric motion models together with HOS-based techniques can be studied. Thus, the strategy consisting in using past frames to obtain low variance estimates could be better exploited.

- The inclusion of the blurring filter in the degradation scheme could be considered. Recall from the general framework introduced in chapter 2 that the general equation was simplified for the case of no blurring. It would be interesting to analyze the behavior of the cost functions in this situation.

- The model employed in this thesis for the motion estimation problem should be verified with real sequences. As we have mentioned in Chapter 4, image frames obtained from surveillance cameras as well medical images may follow such model. The model of other degraded sequences should also be investigated.

- Finally, another area where HOS-based methods can be applied implies images affected by speckled noise. It can be easily shown that the use of HOS in this area is well motivated. HOS-based methods have already been used to restore images degraded by such type of noise [Wear, 1990]. It would be interesting to study the motion estimation problem for sequences affected by speckle noise.

Appendix A

Given a sequence of S images, the Bispectrum of $A\theta(\xi)$ is estimated from $G\theta(\xi) = A\theta(\xi) + N_\theta(\xi) = H\theta(\xi)\, F\theta(\xi) + N_\theta(\xi)$ as the average in (1). $N_\theta(\xi)$ is the FT of the projection of the noise that we assume to be zero-mean, $E\{N_\theta(\xi)\} = 0$, and symmetrically distributed, that is $E\{N_\theta(\xi_1)\, N_\theta(\xi_2)\, N_\theta^*(\xi_1 + \xi_2)\} = 0$. Thus, the statistical expectation of the estimation is

$$E\{\hat{B}a\theta(\xi 1,\xi 2)\} = E\left\{\frac{1}{S}\sum_{i=1}^{S} G\theta_i(\xi 1)\, G\theta_i(\xi 2)\, G\theta_i{}^*(\xi 1+\xi 2)\right\} =$$

$$Ba\theta(\xi 1,\xi 2) + \frac{1}{S}\sum_{i=1}^{S} A_\theta(\xi 1)\; E\{e^{-j\tau i\xi 1}\}\, E\{N_{\theta i}(\xi 2)\, N_{\theta i}{}^*(\xi 1+\xi 2)\} +$$

$$\frac{1}{S}\sum_{i=1}^{S} A_\theta(\xi 2)\; E\{e^{-j\tau i\xi 2}\}\, E\{N_{\theta i}(\xi 1)\, N_{\theta i}{}^*(\xi 1+\xi 2)\} +$$

$$\frac{1}{S}\sum_{i=1}^{S} A_\theta{}^*(\xi 1+\xi 2)\; E\{e^{j\tau i(\xi 1+\xi 2)}\}\, E\{N_{\theta i}(\xi 1)\, N_{\theta i}(\xi 2)\}. \qquad \text{(A1)}$$

where the linear phase factor is a consequence of the shift of observation i. Denoting by $S(\xi_1,\xi_2) = E\{N_{\theta i}(\xi_1)\, N_{\theta i}(\xi_2)\}$, (A1) simplifies to :

$$Ba\theta(\xi 1,\xi 2) + \frac{1}{S}A_\theta(\xi 1)\sum_{i=1}^{S} E\{e^{-j\tau i\xi 1}\}\, S(\xi 2,-\xi 1-\xi 2) +$$

$$\frac{1}{S}A_\theta(\xi 2)\sum_{i=1}^{S} E\{e^{-j\tau i\xi 2}\}\, S(\xi 1,-\xi 1-\xi 2) +$$

$$\frac{1}{S}A_\theta{}^*(\xi 1+\xi 2)\sum_{i=1}^{S} E\{e^{j\tau i(\xi 1+\xi 2)}\}\, S(\xi 1,\xi 2). \qquad \text{(A2)}$$

If τ_i is a random variable uniformly distributed between -T and +T, then $E\{e^{-j\tau i\xi}\} = T\,\mathrm{sinc}(T\xi)$; if it has a triangular distribution then $E\{e^{-j\tau i\xi}\} = 1/4\; T^2\,\mathrm{sinc}^2(T\xi/2)$. Thus for T>>

$$E\{e^{-j\tau i\xi}\} = \begin{cases} 1 & \xi \approx 0 \\ 0 & otherwise \end{cases} \qquad \text{(A3)}$$

Finally we obtain,

$E\{\hat{B}a\theta(\xi 1,\xi 2)\} =$

$$\begin{cases} Ba\theta(\xi 1,\xi 2)+A_\theta(\xi 1)S(\xi 2,-\xi 1-\xi 2)+A_\theta(\xi 2)S(\xi 1,-\xi 1-\xi 2)+A_\theta^{*}(\xi 1+\xi 2)S(\xi 1,\xi 2) & \xi 1\ \xi 2 \approx 0 \\ Ba\theta(\xi 1,\xi 2) & otherwise \end{cases}$$

(A4)

Therefore the Estimation of the Bispectrum is biased near the origin. However the phase is zero at the origin and thus the estimated phase is unbiased except for a small region around the origin. So far we have only assumed that the noise is symmetrically distributed. If it is also white, $S(\xi_1,\xi_2) = N\sigma_n^2\delta(\xi_1+\xi_2)$, where N is the length of the of the observations and σ_n^2 is the variance of the noise, then it is biased only in the axis $\xi_1 = 0$, $\xi_2 = 0$, and $\xi_1+\xi_2=0$:

$$E\{\hat{B}a\theta(\xi 1,\xi 2)\}=\begin{cases} Ba\theta(\xi 1,\xi 2)+A_\theta(\xi 1)\delta(\xi 1)+A_\theta(\xi 2)\delta(\xi 2)+A_\theta^{*}(\xi 1+\xi 2)\delta(\xi 1+\xi 2) & \xi 1\ \xi 2 \approx 0 \\ Ba\theta(\xi 1,\xi 2) & otherwise \end{cases}$$

(A4)

Furthermore, for zero-mean signals $A_\theta(0) = 0$ the estimation is asymptotically unbiased at all frequency pairs.

Appendix B

The 2-D Discrete Fourier Transform of an NxN 2-D signal $f(n_1,n_2)$, is defined as :

$$F(w1,w2) = \sum_{n1=0}^{N-1} \sum_{n2=0}^{N-1} f(n1,n2)\, e^{-jw_1 n_1}\, e^{-jw_2 n_2}$$

denoting by,

$$x(w1,n2) = \sum_{n1=0}^{N-1} f(n1,n2)\, e^{-jw_1 n_1}$$

then

$$F(w1,w2) = \sum_{n2=0}^{N-1} x(w1,n2)\, e^{-jw_2 n_2}$$

$F(w_1,w_2)$ and $x(w_1,n_2)$ can be seen as a 1-D Fourier pair with parameter w_1. Therefore Applying Theorem 1 we can obtain $x(w_1,n_2)$ from the phase of $F(w_1,w_2)$ at any N-1 distinct w_2 frequencies. Analogously, we can see $x(w_1,n_2)$ and $f(n_1,n_2)$ as a 1-D Fourier pair with parameter n_2, and thus recover $f(n_1,n_2)$ from the phase of $x(w_1,n_2)$ at any N-1 distinct w_1 frequencies. Hence, (N-1)(N-1) points of the phase of $F(w_1,w_2)$ in $0 < w_1 < \pi$, $0 < w_2 < \pi$ are needed to reconstruct $f(w_1,n_2)$.

Since w_1 has been used as a fixed parameter in the first place, the pairs (w_1,w_2) are not arbitrarily taken. Although w_1 could be placed at any N-1 distinct frequencies, they must remain the same for any w_2. Thus, the grid of frequencies (w_1,w_2) forms N-1 aligned columns in w_1, of N-1 points arbitrarily distributed in w_2.

Obviously the.same arguments could be reached interchanging w_1 by w_2.

Appendix C

In this appendix we obtain $E\{f_k^2(m)f_k^2(m\text{-}D)\}$, $E\{f_k^3(m)f_k(m\text{-}D)\}$ and $E\{f_k(m)f_k^3(m\text{-}D)\}$, where $D = d\text{-}d_k^o$. The signal is generated as the output of a first order, zero mean Autoregresive (AR) process. For the sake of simplicity we derive these moments for *1-D* signals. Thus:

$$f_k(m) = x_k(m) + b_m f_k(m\text{-}1) \tag{C-1}$$

where $x_k(m)$ is a stationary zero-mean input sequence that is independent of past outputs. The system uses one recent output and the current input to generate the output.

The goal is to derive expressions as a function of the variance, fourth-order moments of the signal and parameters of the model.

For $D=0$ the three moments are equivalent to the fourth-order moment of the signal, that is,

$$m_{f4} = E\{f_k^4(m)\} \tag{C-2}$$

We also define the variance of the signal and the input sequence as $\sigma_f^2 = E\{f_k^2(m)\}$ and $\sigma_x^2 = E\{x_k^2(m)\}$ respectively. We rewrite σ_x^2 in terms of σ_f^2 using C-1, that is,

$$E\{f_k^2(m)\} = E\{x_k^2(m)\} + b_m^2 E\{f_k^2(m\text{-}1)\}$$

Therefore

$$\sigma_x^2 = \sigma_f^2 - b_m^2 \sigma_f^2 \tag{C-3}$$

We derive the kurtosis of the input signal γ_x, in terms of σ_f^2 and m_{f4}, thus using C-1,

$$E\{f_k^4(m)\} = E\{x_k^4(m)\} + b_m^4 E\{f_k^4(m\text{-}1)\} + 6\, E\{x_k^2(m)\} b_m^2 E\{f_k^2(m\text{-}1)\}$$

$$m_{f4} = m_{x4} + b_m^4 m_{f4} + 6\, \sigma_x^2 b_m^2 \sigma_f^2$$

$$m_{x4} - 3\, \sigma_x^4 = m_{f4} - b_m^4 m_{f4} - 6\, b_m^2 \sigma_f^2 (\sigma_f^2 - b_m^2 \sigma_f^2) - 3\, (\sigma_f^2 - b_m^2 \sigma_f^2)^2$$

$$\gamma_x = (m_{f4} - 3\, \sigma_f^4)\,(1\text{-}b_m^4) \tag{C-4}$$

Next we evaluate the three moment functions separately. First, recall that the Barlett-Brillinger-Rosenblatt summation formula, [Brillinguer, 1967] relates the mth-order cumulants of $\{f_k^2(m)\}$ with the impulse response of the system

$$C_{m,f}(\iota_1, \iota_2, \ldots, \iota_{m-1}) = \gamma_x \sum_{n=0}^{\infty} \prod_{j=0}^{m-1} h(n+\iota_j) \tag{C-5}$$

Given (C-1) the impulse response of the system is: $h(n) = b_m{}^n$ for $n \geq 0$. In the following derivations we also utilize the equation that relates cumulants with moments in (2.10), that we repeat here for the discrete signal $f_k(m)$:

$$\begin{aligned} C_{4,f}(\iota_1,\iota_2,\iota_3) = & E\{f_k(m)f_k(m+\iota_1)f_k(m+\iota_2)f_k(m+\iota_3)\} \\ & - E\{f_k(m)f_k(m+\iota_1)\}E\{f_k(m+\iota_2)f_k(m+\iota_3)\} - \\ & - E\{f_k(m)f_k(m+\iota_2)\}E\{f_k(m+\iota_1)f_k(m+\iota_3)\} - \\ & - E\{f_k(m)f_k(m+\iota_3)\}E\{f_k(m+\iota_1)f_k(m+\iota_2)\}. \end{aligned} \quad \text{(C-6)}$$

A) $E\{f_k^2(m)f_k^2(m-D)\}$, it this case $\iota_1 = 0$, $\iota_2 = -D$, $\iota_3 = -D$ in (C-6), thus we obtain

$$E\{f_k^2(m)f_k^2(m-D)\} = C_{4,f}(0,-D,-D) + E\{f_k^2(m)\}E\{f_k^2(m-D)\} + 2\,E^2\{f_k(m)f_k(m-D)\} \quad \text{(C-7)}$$

From C-5 we compute the first term for negative D:

$$C_{4,f}(0,-D,-D) = \gamma_x{}^4 \sum_{n=0}^{\infty} h(n)\, h(n)\, h(n-D)\, h(n-D)$$

$$C_{4,f}(0,-D,-D) = (m_{f4} - 3\,\sigma_f{}^4)\,(1-b_m{}^4) \sum_{n=0}^{\infty} (b_m)^{2n}\,(b_m)^{2(n-D)}$$

Since $\sum_{n=0}^{\infty} (b_m)^{2n}(b_m)^{2(n-D)} = (b_m)^{2(-D)} \dfrac{1}{(1-b_m{}^4)}$ for $-D > 0$ we obtain :

$$C_{4,f}(0,-D,-D) = (m_{f4} - 3\,\sigma_f{}^4)\,(b_m)^{2(-D)} \quad \text{(C-8)}$$

Given the impulse response we obtain the last term in (C-7):

$$\begin{aligned} E\{f_k(m)f_k(m-D)\} &= E\{\sum_{n=0}^{\infty} h(n)\, x(m-n) \sum_{n'=0}^{\infty} h(n')\, x(m-D-n')\} \\ &= \sum_{n=0}^{\infty} \sum_{n'=0}^{\infty} h(n)\, h(n')\, E\{x(m-n)x(m-D-n')\} \\ &= \sum_{n=0}^{\infty} \sum_{n'=0}^{\infty} h(n)\, h(n-D)\, \sigma_x{}^2 \end{aligned}$$

solving the summation and using (C-3) this equation becomes:

$$E\{f_k(m)f_k(m-D)\} = (b_m)^{(-D)}\,\sigma_f{}^2 \quad \text{(C-9)}$$

Finally, using (C-8) and (C-9) in (C-7) we obtain:

$$E\{f_k^2(m)f_k^2(m-D)\} = m_{f4}\,(b_m)^{2(-D)} + \sigma_f{}^4 - (b_m)^{2(-D)}\,\sigma_f{}^4$$

where the second term was substituted by the variance of the signal to the square. For $-D < 0$ the results are the same since $E\{f_k^2(m)f_k^2(m+D)\} = E\{f_k^2(m)f_k^2(m-D)\}$, therefore we rewrite the above equation as :

$$E\{f_k^2(m)f_k^2(m-D)\} = m_{f4}\,(b_m)^{2|D|} + \sigma_f^4 - (b_m)^{2|D|}\,\sigma_f^4 \qquad \text{(C-10)}$$

B) $E\{f_k(m)f_k^3(m-D)\}$, that is, $t_1 = -D$, $t_2 = -D$, $t_3 = -D$ in (C-6), thus we obtain

$$E\{f_k(m)f_k^3(m-D)\} = C_{4,f}(-D,-D,-D) + 3E\{f_k(m)f_k(m-D)\}E\{f_k^2(m-D)\} \qquad \text{(C-11)}$$

Likewise we compute each term, the first one being :

$$C_{4,f}(-D,-D,-D) = \gamma_x^4 \sum_{n=0}^{\infty} h(n)\,h(n-D)\,h(n-D)\,h(n-D)$$

$$C_{4,f}(-D,-D,-D) = (m_{f4} - 3\,\sigma_f^4)\,(1-b_m^4) \sum_{n=0}^{\infty} (b_m)^n\,(b_m)^{3(n-D)}$$

Since $\sum_{n=0}^{\infty} (b_m)^n (b_m)^{3(n-D)} = (b_m)^{3(-D)} \dfrac{1}{(1-b_m^4)}$ for $-D > 0$ we obtain :

$$C_{4,f}(-D,-D,-D) = (m_{f4} - 3\,\sigma_f^4)\,(b_m)^{3(-D)} \qquad \text{(C-12)}$$

The second term was obtained in (C-9), therefore

$$E\{f_k(m)f_k(m-D)\}E\{f_k^2(m-D)\} = (b_m)^{(-D)}\,\sigma_f^2\,\sigma_f^2$$

Finally (C-11) becomes :

$$E\{f_k(m)f_k^3(m-D)\} = (m_{f4} - 3\,\sigma_f^4)\,(b_m)^{3(-D)} + 3(b_m)^{(-D)}\,\sigma_f^4 \qquad \text{(C-13)}$$

This expression is valid for $-D>0$. Let's compute the moment $E\{f_k^3(m)f_k(m-D)\}$ for $-D>0$ and, since $E\{f_k(m)f_k^3(m+D)\} = E\{f_k^3(m)f_k(m-D)\}$ we will derive (C-11) for $-D<0$.

C) $E\{f_k^3(m)f_k(m-D)\}$, we use $t_1 = 0$, $t_2 = 0$, $t_3 = -D$ in (C-6), thus we obtain

$$E\{f_k^3(m)f_k(m-D)\} = C_{4,f}(0,0,-D) + 3E\{f_k(m)f_k(m-D)\}E\{f_k^2(m)\} \qquad \text{(C-14)}$$

Developing the first term we get:

$$C_{4,f}(0,0,-D) = \gamma_x^4 \sum_{n=0}^{\infty} h(n)\,h(n)\,h(n)\,h(n-D)$$

$$C_{4,f}(0,0,-D) = (m_{f4} - 3\,\sigma_f^4)\,(1-b_m^4) \sum_{n=0}^{\infty} (b_m)^{3n}\,(b_m)^{(n-D)}$$

Since $\sum_{n=0}^{\infty} (b_m)^{3n}(b_m)^{(n-D)} = (b_m)^{(-D)} \frac{1}{(1-b_m^4)}$ for $-D > 0$ we obtain :

$$C_{4,f}(0,0,-D) = (m_{f4} - 3\,\sigma_f^4)\ (b_m)^{(-D)} \tag{C-15}$$

Finally (C-14) becomes :

$$E\{f_k^3(m)f_k(m-D)\}=(m_{f4} - 3\,\sigma_f^4)\ (b_m)^{(-D)} + 3(b_m)^{(-D)}\,\sigma_f^4$$

$$E\{f_k^3(m)f_k(m-D)\}= m_{f4}\,(b_m)^{(-D)} \tag{C-16}$$

If we define

$$\Gamma_f(b_m,D) = (m_{f4} - 3\,\sigma_f^4)\ (b_m)^{3|D|} + 3(b_m)^{|D|}\,\sigma_f^4 \tag{C-17}$$

and

$$\Psi_f(b_m,D) = b_m^{|D|}\,m_{f4} \tag{C-18}$$

the above definitions yield to :

$$E\{f_k(m)f_k^3(m-D)\}=\begin{cases} \Psi_f(b_m,D) & D>0 \\ \Gamma_f(b_m,D) & D<0 \end{cases} \tag{C-19}$$

It's straightforward to see also that,

$$E\{(f_k^3(m)f_k(m-D)\} = \begin{cases} \Gamma_f(b_m,D) & D>0 \\ \Psi_f(b_m,D) & D<0 \end{cases} \tag{C-20}$$

Appendix D

In this appendix we derive the new cost functions in terms of the signal and the noise moments. The cost functions prior to normalization are given by:

$$J_{42k}(d) = E\{DFD_k^4(d)\} - 3\,E\{DFD_k^2(d)\}E\{DFD_{k-1}^2(d)\} \quad \text{(D-1)}$$

$$J_{43k}(d) = E\{DFD_k^4(d)\} - 3\,E\{DFD_k^2(d)\}E\{DFD_0^2(d)\} \quad \text{(D-2)}$$

where

$$E\{DFD_0^2(d)\} = E\{[g_k(m)-g_k(m-d)]\} \quad \text{(D-3)}$$

A) We first analyze J_{42k}. For this purpose we decompose $DFD_k(d)$ in noise and signal differences. Thus, the first term of $J_{42k}(d)$ in (D-1) becomes:

$$E\{DFD_k^4(d)\} = E\{DSD_k^4(d)\} + E\{DND_k^4(d)\} + 6\,E\{DND_k^2(d)\,DSD_k^2(d)\}$$
$$+4\,E\{DND_k(d)\,DSD_k^3(d)\} + 4\,E\{DND_k^3(d)DSD_k(d)\} \quad \text{(D-4)}$$

The last two terms cancel out according to the assumption that the signal is independent from the noise and both are zero-mean signals. This yields,

$$E\{DFD_k^4(d)\} = E\{DSD_k^4(d)\} + E\{DND_k^4(d)\} + 6\,E\{DND_k^2(d)\,DSD_k^2(d)\} \quad \text{(D-5)}$$

For the second term of $J_{42k}(d)$ we obtain

$$E\{DFD_k^2(d)\}\,E\{DFD_{k-1}^2(d)\} = [E\{DSD_k^2(d)\}+E\{DND_k^2(d)\}+2E\{DND_k(d)\,DSD_k(d)\}]\cdot$$
$$[E\{DSD_{k-1}^2(d)\}+E\{DND_{k-1}^2(d)\}+2E\{DND_{k-1}(d)DSD_{k-1}(d)\}]$$
$$=[E\{DSD_k^2(d)\}+E\{DND_k^2(d)\}]\,[E\{DSD_{k-1}^2(d)\}+E\{DND_{k-1}^2(d)\}]\,, \quad \text{(D-6)}$$

where the same assumptions were applied. Substituting (D-6) and (D-7) in (D-1),

$$J_{42k}(d) = E\{DSD_k^4(d)\} + E\{DND_k^4(d)\} + 6E\{DSD_k^2(d)\}E\{DND_k^2(d)\}$$
$$- 3E\{DSD_k^2(d)\}E\{DSD_{k-1}^2(d)\} - 3E\{DSD_k^2(d)\}E\{DND_{k-1}^2(d)\}$$
$$-3E\{DSD_{k-1}^2(d)\}E\{DND_k^2(d)\} - 3E\{DND_k^2(d)\}E\{DND_{k-1}^2(d)\}. \quad \text{(D-7)}$$

Since we can consider that the noise differences have the same statistics at time k and $k-1$, $E\{DND_k^2(d)\} = E\{DND_{k-1}^2(d)\}$, the terms corresponding to the kurtosis of the noise cancel out (second and last terms), and the cost function simplifies to:

$$J_{42k}(d) = E\{DSD_k^4(d)\} + 3E\{DSD_k^2(d)\}E\{DND_k^2(d)\}$$

$$- 3E\{DSD_k^2(d)\}E\{DSD_{k-1}^2(d)\}-3E\{DSD_{k-1}^2(d)\}E\{DND_k^2(d)\} \quad \text{(D-8)}$$

This equation can be rewritten as:

$$J_{42k}(d) = E\{DSD_k^4(d)\} - 3E\{DSD_k^2(d)\}E\{DSD_{k-1}^2(d)\}$$
$$-3E\{DND_k^2(d)\}[E\{DSD_{k-1}^2(d)\}-E\{DSD_k^2(d)\}] \quad \text{(D-9)}$$

Using the expressions that were derived in Chapter 4

$$E\{DND_k^2(d)\} = 2\sigma_n^2 - 2r_{n1}(d)$$

$$E\{DSD_k^2(d)\} = 2\sigma_f^2 - 2r_f(d-d_k^o)$$

$$E\{DSD_{k-1}^2(d)\} = 2\sigma_f^2 - 2r_f(d-d_{k-1}^o)$$

$$E\{DSD_k^4(d)\} = 2m_{f4} + 6E\{f_k^2(m)f_k^2(m+d_k^o-d)\}$$
$$-4E\{f_k^3(m)f_k(m+d_k^o-d)\} - 4E\{f_k(m)f_k^3(m+d_k^o-d)\} \quad \text{(D-10)}$$

we finally obtain:

$$J_{42k}(d) = 2m_{f4} + 6E\{f_k^2(m)f_k^2(m+d_k^o-d)\}$$
$$-4E\{f_k^3(m)f_k(m+d_k^o-d)\} - 4E\{f_k(m)f_k^3(m+d_k^o-d)\}$$
$$-3[2\sigma_f^2 - 2r_f(d_k^o-d)][2\sigma_f^2 - 2r_f(d_{k-1}^o-d)] - 3[2\sigma_n^2 - 2r_n(d)][2r_f(d_{k-1}^o-d) - 2r_f(d_k^o-d)] \quad \text{(D-11)}$$

for an uncorrelated signal the above equation becomes:

$$J_{42k}(d) = \begin{cases} 2m_{f4} - 6\sigma_f^2 & d \neq d_k^o \neq d_{k-1}^o \\ 6\sigma_f^2[2\sigma_n^2 - 2r_n(d)] & d = d_k^o \neq d_{k-1}^o \\ -2m_{f4} - 6\sigma_f^2 + 6\sigma_f^2[2\sigma_n^2 - 2r_n(d)] & d = d_{k-1}^o \neq d_k^o \\ 0 & d = d_k^o = d_{k-1}^o \end{cases}$$

(D-12)

which is the result used in that Chapter

B) In second place we analyze $J_{43k}(d)$ as a function of signal and noise moments, using (D-6) for the fourth-order moment of the $DFD_k(d)$:

$$J_{43k}(d) = E\{DSD_k^4(d)\} + E\{DND_k^4(d)\} + 6E\{DSD_k^2(d)\}E\{DND_k^2(d)\}$$
$$-3[E\{DSD_0^2(d)\} + E\{DND_0^2(d)\}][E\{DSD_k^2(d)\} + E\{DND_k^2(d)\}] \quad \text{(D-13)}$$

where

$$E\{DND_0^2(d)\} = 2\sigma_n^2 - 2r_{n0}(d)$$

$$E\{DSD_0^2(d)\} = 2\sigma_f^2 - 2r_f(d) \tag{D-14}$$

Using the above expressions and (D-10)

$$\begin{aligned}
J_{43k}(d) = {} & 2m_{f4} + 6E\{f_k^2(m) f_k^2(m+d_k^o-d)\} \\
& -4E\{f_k^3(m) f_k(m+d_k^o-d)\} - 4E\{f_k(m) f_k^3(m+d_k^o-d)\} \\
& -3[2\sigma_n^2 - 2r_{n1}(d)]^2 \\
& +6[2\sigma_f^2 - 2r_f(d-d_k^o)][2\sigma_n^2 - 2r_{n1}(d)] \\
& -3[2\sigma_f^2 - 2r_f(d) + 2\sigma_n^2 - 2r_{n0}(d)][2\sigma_f^2 - 2r_f(d-d_k^o) + 2\sigma_n^2 - 2r_{n1}(d)]
\end{aligned} \tag{D-15}$$

where we used $K(DND_k(d)) = E\{DND_k^4(d)\} - 3(E\{DND_k^4(d)\})^2 = 0$

for an uncorrelated signal the cost function becomes,

$$J_{43k}(d) =$$

$$\begin{cases}
2m_{f4} + 6\sigma_f^4 - 12[\sigma_n^2 - r_{n1}(d)]^2 + 24\sigma_f^2[\sigma_n^2 - r_{n1}(d)] - 12[\sigma_f^2 + \sigma_n^2 - r_{n0}(d)][\sigma_f^2 + \sigma_n^2 - r_{n1}(d)] & d \neq d_k^o \neq 0 \\
-12[\sigma_n^2 - r_{n1}(d_k^o)]^2 - 12[\sigma_f^2 - r_f(d_k^o) + \sigma_n^2 - r_{n0}(d_k^o)][\sigma_n^2 - r_{n1}(d)] & d = d_k^o \neq d_{k-1}^o \\
2m_{f4} + 6\sigma_f^4 - 12[\sigma_n^2 - r_{n1}(0)]^2 - 12[\sigma_f^2 - r_f(-d_k^o)][\sigma_n^2 - r_{n1}(0)] & d = 0 \neq d_k^o \\
0 & d = d_k^o = 0
\end{cases} \tag{D-16}$$

which corresponds to the result used in Chapter 4.

References

J. K. Aggarwal and N. Nandhakumar," On the computation of Motion from Sequences of Images-A Review", *Proceedings of the IEEE* , Vol. 76(8)pp. 917-935, August **1988.**

P. O. Amblard, J. L. Lacoume and J. M. Brossier," Transient detection, Higher-Order Time Frequency distributions and the Entropy", *IEEE SPWorkshop on HOS,* Lake Tahoe, CA, pp. 265-269, June **1993.**

P. Anandan, J. R. Bergen and K.J. Hanna, "Hierarchical Model-Based Motion Estimation", *in Image Sequence Analysis,* Sezan and Lagendijk Editors, Kluwer academic publishers, **1993.**

J. M. Anderson and G. B. Giannakis, "Image Motion Estimation Algorithms Using cumulants", *To appear in IEEE Transactions on Image Processing,* **1994.**

J. M. Anderson and G. B. Giannakis, "Noise Insensitive Image Motion Estimation Algorithms Using cumulants", *Proceedings of ICASSP '91*, Toronto, pp. 2721-2724, **1991.**

H.C. Andrews and B. R. Hunt, "*Digital Image Restoration*", Englewood Cliffs,NJ: Prentice Hall, pp. 144, **1979.**

H. Bartelt, A. W. Lohmann and B. Wirnitzer, "Phase and Amplitude recovery from bispectra", *Applied Optics,* vol. 23, pp. 3121-3129, September **1984.**

H. C. Bergmann, "Displacement Estimation Based on the Correlation of Image Sequences",*Proceedings of IEE Int. Conf. on Electronic Image Processeing,* pp. 215-219, **1982.**

M. Bertero, T. Poggio and V. Torre, "Ill-posed problems in early vision",*Proceedings of IEEE,* vol. 76, pp. 869-889, September **1984.**

D. R. Brillinger and M. Rosenblatt, "Computation and interpretation of kth-order spectra", *in B. Harris editor, spectral analysis of time series,* Wiley, NY, pp. 189-232, **1967.**

D. R. Brillinger, "Introduction to polyspectra", *Annals Math. Stat.*, vol. 36, pp. 1351-1374, **1965**.

C. Cafforio and F. Rocca, "Methods for Measuring Small Displacements of Television Images", *IEEE Transactions on Information Theory*, Vol. 22, No. 6, pp. 573-579, September **1976**.

CCITT Subgrup 15, Working Partyh 15/1 Specialists Group on Coding for Visual Telephony, **1990**.

V. Chandran and S. Elgar, "Position, rotation, and scale invariant recognition of images using Higher-order spectra", *Proceedings of ICASSP '92*, San Francisco, pp. v-213-216, **1992**.

V. Chandran and S. Elgar, "Pattern Recognition Using Invariants Defined from Higher Order Spectra-One Dimensional Inputs", *IEEE Transactions on Signal Processing*, Vol 41, No 1, pp.205-212, January **1993**.

C.K Cheong, K. Aizawa, T. Saito and M. Hatori, "Motion Estimation with Wavelet Transform and the application to motion compensated interpolation", *Proceedings of ICASSP '93*, Minneapolis, pp. v-217-220, **1993**.

J. C. Dainty, " Bispectrum Imaging through Turbulence", *Workshop on HOS Analysis*, Vail, Colorado, pp. 130-133, June **1989**.

S.R. Deans, "*The Radon Transform and some of its applications*", Wiley- Interscience, **1983**.

S. A. Dianat and M. R. Raghuveer, "Fast Algorithms for phase and magnitude reconstruction from bispectra", *Optical Engineering*, Vol 29 No. 5, pp. 504-512, May **1990**.

J.N. Driessen, J. Biemond and D. E. Boekee, " A Pel-Recursive Segmentation and Estimation Algorithm for Motion Compensated Image Sequence Coding", *Proceedings. IEEE ICASSP'89*, pp. 1901-1904, Glasgow, Scotland, April **1989**.

S. A. Dianat and M. R. Raghuveer, " Two-Dimensional Non-Minimum Phase Signal Reconstruction", *Workshop on HOS Analysis*, Vail, Colorado, pp. 112-116, June **1989**.

J. C. Dudgeon, " The existence of Cepstra for Two-Dimensional Rational Polynomials", *IEEE Transactions on ASSP*, pp. 242-243, April **1975**.

S. N. Efstratiadis, "Adaptive Constrained Recursive Motion Field and Image Sequence Estimation", *PhD Thesis*, Northwestern University, **1991**.

A. T. Erdem and M. Tekalp,"Blur Identification using the Bispectrum", *Proceedings of ICASSP '90*, Alburquerque, NM, pp. 1961-1964, **1990**.

C.L. Fennema and W.B. Thompson, "Velocity determination in Scenes Containing several moving objects", *Computer Vision, Graphics, Image Processing,* vol. CVGIP-9, pp 301-315, **1979**.

J.A. Fonollosa and J. Vidal, "System Identification using a linear combination of cumulant slices", *IEEE Transactions on Signal Processing,* Vol 41, No 7, pp. 2405-2412, July **1993**.

G. B. Giannakis, "Signal Reconstruction from Multiple Correlations: frequency- and time-domain approaches", *Journal Opt.ical Society of America*, Vol. 6, No. 5, May **1989**.

Joseph Goodman, "*Statistical Optics*", Wiley- Interscience, **1985**.

T. E. Hall and G. B. Giannakis, "Bispectral Analysis and Model Validation of texture Images", *Submitted to IEEE Transactions on Image Processing,* **1993**.

M. H. Hayes, J. S. Lim and A. V. Oppenheim, "Signal Reconstruction from the phase or magnitude", *IEEE on ASSSP*, Vol. 28, No. 6, pp. 672-680, December **1980**.

M. V. Hinich, "Detecting a Transient Signal by Bispectral Analysis", *IEEE Transactions on ASSP,* Vol. 38, No. 7, pp. 1277-1283, July **1990**.

K. H. Hofmann and G. Weigelt, " Astronomical speckle masking: image reconstruction by cross triple correlation", *Applied Optics*, Vol. 26, No 10,pp. 2011-2015, December **1983**.

K. P. Horn and B. G. Schunk, " Determining Optical Flow", *Artificial Intelligence*, Vol. 17,pp. 185-203, **1981**.

T.S. Huang, " Some notes on film grain noise", NASA Summer study on Atmospheric Degradations, Woods Hole, Mass, **1968**.

T.S. Huang, editor,*" Image Sequence Analysis"*, Springer-Verlag, **1981a**.

T.S. Huang and R. Y. Tsai, " Image Sequence Analysis: Motion Estimation", in *Image Sequence Analysis*, T.S. Huang, editor, pp. 104-124, Springer-Verlag, **1981b**.

G. Jacovitti, " Applications of Higher Order Statistics in Image Processing", *Proceeedings of the International Signal Processing Workshop on HOS* , Chamrousse, France, pp. 241-247, July **1991**.

A. K. Jain, "Advances in Mathematical Models for Image Processing",*Proceedings of IEEE*, vol. 69, no. 5, pp. 502-528, May **1981a**.

J. R. Jain and A. K. Jain, "Displacement Measurements and Its Application in Interframe Image Coding", *IEEE Transactions on Communications*, Vol. 29(12), pp. 1799-1808, December **1981b**.

A. K. Jain, *"Fundamentals of Digital Image Processing"*, Prentice-Hall Inc., **1989**.

M.G.Kang, K.T.Lay and A.K. Katsaggelos, " Phase Estimation using the Bispectrum and its application to image restoration", *Optical Engineering*, Vol. 30, No 7, pp. 976-985, July **1991**.

A.K. Katsaggelos editor, " *Digital Image Restoration*", Springer Series in INformation Sciences, **1991**.

R. P. Kleihorst, R. L. Lagendijk and J. Biemond, "Noise reduction of severely corrupted images", *Proceedings of ICASSP '93*, Minneapolis, pp. v293-96, **1993**.

A. Kojima, N. Sakurai and J. Kishigami, "Motion Estimation using 3D-FFT Spectrum", *Proceedings of ICASSP '93*, Minneapolis, pp. v-213-216, **1993**.

J. Konrad and E. Dubois, "Estimation of Image fields", *Proceedings of IEEE ICASSP '88*, New York City, NY, pp. 1072-1075, **1988**.

A. Labeyrie, " Atteinment of Diffraction Limited Resolution in Large Telescopes by Fourier Analysing Speckle Patterns in Star Images", *Astronomy & Astrophysics*, Vol. 6, No 1, pp. 85-87, January **1970**.

J. O. Limb and J. A. Murphy, "Measuring the Speed of Moving Objects from Television Signals", *IEEE Transactions on Communications*, Vol. 23, No. 4, pp. 474-478 April **1975**

R. Pan and C. L. Nikias, "The Complex Cepstrum of Higher-Order Cumulants and Nonminimum Phase System Identification", *IEEE Transactions on ASSP*, Vol. 36, No. 2, pp. 186-205, February **1988**.

A. Papoulis, *"Probablity, Random Variables, and Stochastic Processes"*, McGraw-Hill Inc., Second Edition, **1984**.

A. P. Petropulu and C. L. Nikias, "Signal Reconstruction from the phase of the Bispectrum", *IEEE Transactions on Signal Processing*, Vol. 40, No. 3, pp. 869-890, March **1992**.

W.H. Press, B.P. Flannery, S.A. Teulovsky and W.T. Vetterling, " *Numerical Recipes in C*", Cambridge University Press, **1990**.

D. Rosille, J. Leroux, F. Germain and O. Jourdan, "Speckle masking in the frequency domain: Comparison of several algorithms on actual astrophysical data", *Proceedings of EUSIPCO'94*, Edinbourgh, UK, pp. 117-1120, September **1994**.

B.M.Sadler, "Shift and Rotation Invariant Object Reconstruction using Bispectrum", *Workshop on HOS Analysis*, Vail, Colorado, pp. 106-111, June **1989**.

P. Salembier and M. Pardàs, "Hierarchical Morphological Segmentation and Coding for image sequences", *to appear on the Special issue on Image Sequence Compression, IEEE Transactions on Image Processing*, September **1994**.

E. Sayrol, T. Gasull and J. R. Fonollosa, "Cost Function for motion estimation based on Higher-Order Statistics", *Proceedings of EUSIPCO'94*, Edinbourgh, UK, pp. 117-1120, September **1994**.

E. Sayrol, C. L. Nikias and T. Gasull, "Image Restoration Using the WS", *submitted to the IEEE Transactions on Image Processing* , June **1993**.

E. Sayrol, C. L. Nikias and T. Gasull, "Image Restoration Using Higher-Order Statistics and the Radon Transform", *IEEE Signal Processing Workshop on HOS*, Lake Tahoe, pp. 76-80, California, June **1993**.

E. Sayrol and C. L. Nikias, "Image Restoration Using Projections", *SIPI Annual Research Review, Marina del Rey, CA* , February **1993**.

M.I. Sezan and R. L. Lagendijk Editors, "*Motion Analysis and image sequence processing*", Kluwer academic publishers, **1993**.

M.I. Sezan, G. Pavlovic and M. Tekalp,"On modeling the focus blur on Image restoration", *Proceedings of ICASSP '91*, Toronto, Canada, pp. 2485-2488, **1991.**

M.I. Sezan and M. Tekalp, *"Image Restoration and Reconstruction""*, Optical Engineering, Vol. 29, No. 5, May **1990.**

R. Srinivasan and K. R. Rao, "Predictive Coding Based on Efficient Motion Estimation", *IEEE Transactions on Communications,* Vol. 33, No. 8, pp. 888-896, August **1985.**

C. Stiller, "A statistical Image Model for Motion Estimation", *Proceedings of ICASSP '93*, Minneapolis, pp. v-193-196, **1993.**

G. Sundaramoorthy, M. R. Raghuveer and S. A. Dianat, "Bispectral Reconstruction of Signals in Noise ", *IEEE Transactions on ASSP*, Vol. 38, No 7, July **1990.**

M.Tabei and M. Ueda, "Backprojection by upsampled Fourier series Expansion and Interpolated FFT", *IEEE Transactions on Image Processing*, Vol. 1, No 1, pp. 77-87, January **1992.**

M. Tekalp and A. T. Erdem, "Higher-Order Spectrum Factorization in One and Two Dimensionsions with Applications in Signal Modeling and Non-Minimum Phase Identification", *IEEE Transactions on ASSP,* Vol. 37, No. 10, pp. 1537-1549, **1989.**

M. Tekalp and G. Pavlovic, "Restoration of Scanned Photographic Images" in *Digital Image Restoration*, A.K. Katsaggelos Ed., Springer Series in Information Sciences, **1991.**

M. K. Tsatsanis and G. B. Giannakis, "Translation, rotation and scaling invariant object and texture classification using polyspectra", *Proceedings of SPIE'90,* 1348,pp 103-115, San Diego, Ca, July **1990.**

J. K. Tugnait, "Estimation of Linear Parametric Models of NonGaussian Discrete Random Fields with application to Texture Analysis", *IEEE Transactions on Image Processing*, Vol. 3, No 2, pp. 109-127, March **1994.**

J. K. Tugnait, "Texture Synthesis Using Asymetric 2-D Noncausal AR Models", *IEEE Signal Processing Workshop on HOS*, Lake Tahoe, pp. 71-75, California, June **1993.**

J. K. Tugnait, "Time Delay Estimation in Unknown Spatially Correlated Gaussian Noise Using Higher-Order Statistics", *Proc. 23rd Asilomar Conf. Sig. Sys., Comp.*, pp. 211-215, Pacific Grove, CA, **1989**.

J. Vidal, "Non-Gaussian ARMA Estimation based on Higher-Order Statistics", *Tesis Doctoral*, UPC, **1993**.

T. Viero and Y. Neuvo, "3-D Median Structures for Image Sequence Filtering and Coding", *in Image Sequence Analysis*, Sezan and Lagendijk Editors, Kluwer academic publishers, **1993**.

J.F. Walkup, R.C. Choens, "Image Processing in Signal-Dependent Noise", *To appear in Optical Engineering*, 13, pp. 258-266 **1974**.

S Wear and M.R. Raghuveer, "Bispectral Analysis of Speckled Images", *Proceedings of ICASSP '90*, Alburquerque, NM, pp. 238-241, **1990**.

S.F. Wu and J. Kittler, "General Motion Estimation and Segmentation", *Proceedings of SPIE Conf. Visual Commun. and Image Processing*, vol 1360, pp. 1198-1209, Lausanne, Switzerland, October **1990**.

H. Zheng and Steven D. Blostein, "An Error-Weighted Regularization Algorithm fro Image Morion-Field Estimation", *IEEE Transactions on Image Processing*, Vol. 2, No 2, pp. 246-252, April **1993**.

G. Zhou and G. B. Giannakis, "Cumulant based stationary and nonstationary models for classification and synthesis of random fields", *Proceedings of SPIE'92*, 1348, San Diego, Ca, July **1992**.

G. Zhou and G. B. Giannakis, "On statistical models for classification and synthesis of textures", *To appear in Optical Engineering*, **1994**.